Short article

Cell Host & Microbe

Cytoplasmic calcium influx mediated by plant MLKLs confers TNL-triggered immunity

Graphical abstract

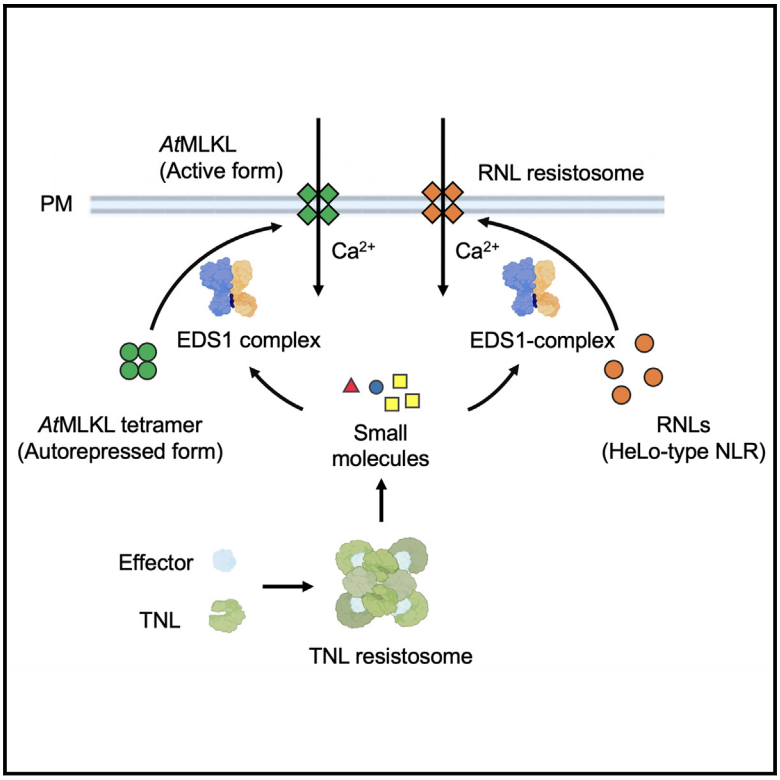

Highlights

- *At*MLKL1 clusters at the plasma membrane on TNL activation in an EDS1-dependent manner
- *At*MLKLs confer immunity in parallel with RPW8-type helper NLRs
- *At*MLKLs promote a sustained $[Ca^{2+}]_{cyt}$ influx after the activation of TNL receptor immunity
- The N-terminal HeLo domain of *At*MLKL1 is responsible for $[Ca^{2+}]_{cyt}$ influx

Authors

Qiaochu Shen, Keiichi Hasegawa, Nicole Oelerich, ..., Jane E. Parker, Jijie Chai, Takaki Maekawa

Correspondence

tmaekawa@uni-koeln.de

In brief

Plant MLKLs promote Toll-interleukin-1 receptor domain NLR (TNL)-triggered immunity. Shen et al. show that, like their animal counterparts, the self-oligomerization of the N-terminal HeLo domain is essential for their functionality and that they mediate sustained cytoplasmic Ca^{2+} influx during TNL- but not CNL-triggered immunity, anticipating an animal MLKL function in regulating Ca^{2+} homeostasis.

Shen et al., 2024, Cell Host & Microbe *32*, 1–13
April 10, 2024
https://doi.org/10.1016/j.chom.2024.02.016

CellPress

Cell Host & Microbe

CellPress
OPEN ACCESS

Short article

Cytoplasmic calcium influx mediated by plant MLKLs confers TNL-triggered immunity

Qiaochu Shen,[1,7] Keiichi Hasegawa,[2,7] Nicole Oelerich,[3] Anna Prakken,[1] Lea Weiler Tersch,[1] Junli Wang,[4] Frowin Reichhardt,[1] Alexandra Tersch,[1] Je Cuan Choo,[1] Ton Timmers,[4] Kay Hofmann,[3] Jane E. Parker,[4,5] Jijie Chai,[2,4,5,6] and Takaki Maekawa[1,5,8,*]

[1]Institute for Plant Sciences, University of Cologne, 50674 Cologne, NRW, Germany
[2]Institute for Biochemistry, University of Cologne, 50674 Cologne, NRW, Germany
[3]Institute for Genetics, University of Cologne, 50674 Cologne, NRW, Germany
[4]Max Planck Institute for Plant Breeding Research, 50829 Cologne, NRW, Germany
[5]Cluster of Excellence on Plant Sciences (CEPLAS), Cologne, NRW, Germany
[6]Present address: School of Life Sciences, Westlake University, Hangzhou 310024, Zhejiang, China
[7]These authors contributed equally
[8]Lead contact
*Correspondence: tmaekawa@uni-koeln.de
https://doi.org/10.1016/j.chom.2024.02.016

SUMMARY

The plant homolog of vertebrate necroptosis inducer mixed-lineage kinase domain-like (MLKL) contributes to downstream steps in Toll-interleukin-1 receptor domain NLR (TNL)-receptor-triggered immunity. Here, we show that *Arabidopsis* MLKL1 (*At*MLKL1) clusters into puncta at the plasma membrane upon TNL activation and that this sub-cellular reorganization is dependent on the TNL signal transducer, EDS1. We find that *At*MLKLs confer TNL-triggered immunity in parallel with RPW8-type HeLo-domain-containing NLRs (RNLs) and that the *At*MLKL N-terminal HeLo domain is indispensable for both immunity and clustering. We show that the *At*MLKL HeLo domain mediates cytoplasmic Ca^{2+} ($[Ca^{2+}]_{cyt}$) influx in plant and human cells, and *At*MLKLs are responsible for sustained $[Ca^{2+}]_{cyt}$ influx during TNL-triggered, but not CNL-triggered, immunity. Our study reveals parallel immune signaling functions of plant MLKLs and RNLs as mediators of $[Ca^{2+}]_{cyt}$ influx and a potentially common role of the HeLo domain fold in the Ca^{2+}-signal relay of diverse organisms.

INTRODUCTION

In plants, a two-layered immune mechanism comprising pathogen-associated molecular pattern (PAMP)-triggered immunity and effector-triggered immunity (ETI)[1–6] effectively detects and combats pathogenic microbes. In many cases, ETI is initiated by intracellular nucleotide-binding leucine-rich repeat (NLR) receptors upon detection of pathogen race-specific effectors.[7,8] Three major classes of plant NLRs—Toll-interleukin-1 receptor domain NLRs (TNLs), CNLs, and RPW8-type NLRs (RNLs)—are defined by the presence of either a Toll/interleukin-1 receptor (TIR)-like domain, a coiled-coil (CC) domain, or an RPW8-like CC domain (also known as a HeLo domain) at the N terminus, respectively.[8–10] Activation of the multi-domain NLRs involves conformational changes leading to the assembly of supramolecular complexes called "resistosomes."[11–15] Activated CNLs such as ZAR1 form pentameric resistosomes, which function as non-selective calcium ion (Ca^{2+})-permeable channels at the plasma membrane (PM).[11,16] By contrast, pathogen-activated TNLs such as *Arabidopsis* RPP1 and *N. benthamiana* Roq1 form tetrameric resistosomes, which have TIR-encoded nicotinamide adenine dinucleotide hydrolase (NADase) activity-producing nucleotide signaling intermediates for defense promotion.[13,17–21] Besides TNLs, plant genomes encode a number of shorter TIR-NB-ARC-domain-containing and TIR-only proteins.[7,22,23] Therefore, TIR-mediated enzymatic activity plays a pivotal role in plant immunity.

The execution of TNL and TIR enzyme-triggered immune signaling requires the lipase-like proteins enhanced disease susceptibility 1 (EDS1), senescence associated gene 101 (SAG101) and phytoalexin deficient 4 (PAD4), and activated disease resistant 1 (ADR1)- or N requirement gene 1 (NRG1)-family RNLs.[24–26] Two sets of non-cyclic ribosylated nucleotide products of the TIR enzymes are bound by two distinct receptors: EDS1-SAG101 and EDS1-PAD4 heterodimer complexes.[27,28] This promotes EDS1-SAG101- and EDS1-PAD4-facilitated conformational changes in ADR1 and NRG1, respectively, leading to their oligomerization.[24–28] Oligomerized RNLs are enriched in puncta on the PM and mediate cytoplasmic Ca^{2+} ($[Ca^{2+}]_{cyt}$) influx in plant and human cells.[29–31] In plant immunity, the signatures of $[Ca^{2+}]_{cyt}$ influx are decoded into distinct downstream outputs, including host cell death.[22,32] We recently showed that the plant homolog of animal necroptosis inducer mixed-lineage kinase domain-like (MLKL) contributes to TNL-triggered immunity.[10]

Please cite this article in press as: Shen et al., Cytoplasmic calcium influx mediated by plant MLKLs confers TNL-triggered immunity, Cell Host & Microbe (2024), https://doi.org/10.1016/j.chom.2024.02.016

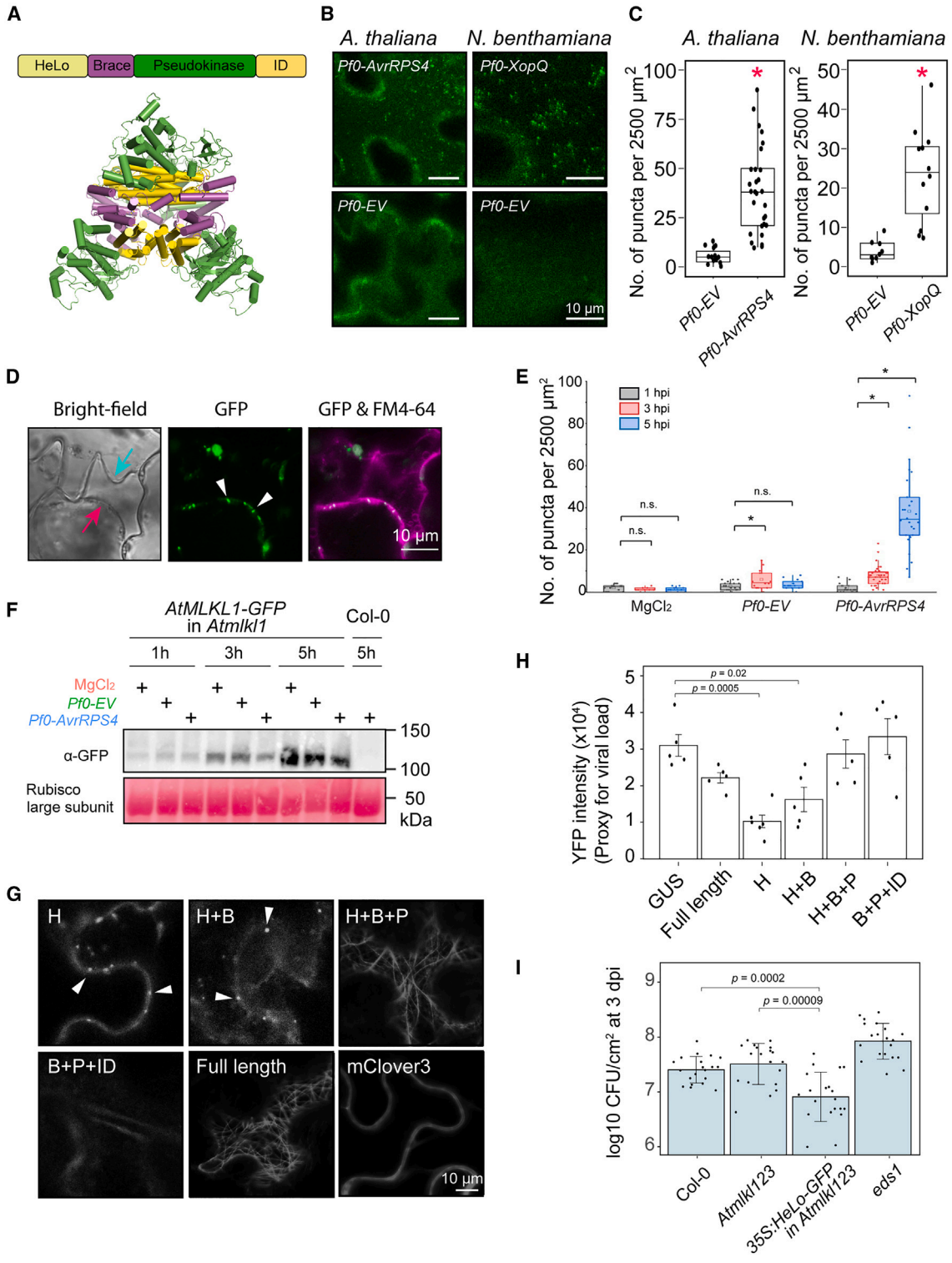

Figure 1. *Arabidopsis* MLKL1 forms clusters at the plasma membrane (PM) during TNL-triggered immunity in a HeLo-domain-dependent manner

(A) Schematic representations of *At*MLKLs. Top: *At*MLKLs consist of four domains. Bottom: cryo-EM structure of a protomer of the *At*MLKL3 tetramer (PDB: 6KA4). Subdomains are shown in different colors. Yellow: HeLo, purple: brace, green: pseudokinase, dark yellow: intrinsically disordered (ID). The ID region does not appear in the cryo-EM structures, likely due to its instability.

(B) Confocal microscopy analysis of leaf epidermis expressing *At*MLKL1-GFP. Left: top-view of leaf epidermal cells of *Arabidopsis* complementation line expressing *At*MLKL1-GFP under the native *cis*-regulatory sequence in *Atmlkl1* background[10] upon challenge with Pf0-AvrRPS4 or Pf0-EV at 5 h post-infiltration

(legend continued on next page)

Please cite this article in press as: Shen et al., Cytoplasmic calcium influx mediated by plant MLKLs confers TNL-triggered immunity, Cell Host & Microbe (2024), https://doi.org/10.1016/j.chom.2024.02.016

Despite their roles in TNL-mediated EDS1-dependent immunity, the functional relationship between RNLs and MLKLs is not known.

Plant MLKLs and RNLs share an N-terminal four-helix bundle in a CC arrangement, which is structurally similar to the N-terminal HeLo domain (named after the fungal heterokaryon incompatibility locus (HET) and loss-of-pathogenicity B (LopB) proteins) of animal MLKL, a lytic cell death inducer.[10,29,33–35] HeLo-domain-containing proteins occur in diverse organisms, exemplified by fungal HET-S[36,37] and a viral MLKL-like protein.[38] Plant and animal MLKLs have an N-terminal HeLo domain, followed by a brace region and a pseudokinase domain.[10,39,40] Plant MLKLs additionally possess a C-terminal intrinsically disordered (ID) region that is missing in animal counterparts.[10] The cryoelectron microscopy (cryo-EM) structures of wild-type *At*MLKLs revealed a tetrameric configuration in which the N-terminal HeLo domains are completely buried (Figure 1A), suggesting that the tetrameric structure represents an auto-repressed configuration of plant MLKLs.[10] However, the mode of MLKL activation and its immune activity remain obscure.

Here, we describe the N-terminal HeLo-domain-dependent clustering of *Arabidopsis* MLKL1 (*At*MLKL1) at the PM upon TNL activation in *Arabidopsis* and *Nicotiana benthamiana*. Genetic and functional studies indicate that *At*MLKLs and RNLs confer TNL-mediated immunity in a parallel manner and that the *At*MLKL N-terminal HeLo domain, which can self-oligomerize, is indispensable for *At*MLKL-mediated immunity. Furthermore, we detect a TNL-activation-dependent interaction between the EDS1-SAG101 dimer and *At*MLKL1, suggesting a mechanistic explanation for the lack of *At*MLKL1 clustering on the PM in an *eds1* null mutant. Finally, we show that the HeLo domain of plant MLKL mediates $[Ca^{2+}]_{cyt}$ influx in plant and human cells and that plant MLKLs facilitate sustained $[Ca^{2+}]_{cyt}$ influx during TNL-triggered immunity but not CNL-triggered immunity.

RESULTS

*At*MLKL1 clusters at the PM during TNL-triggered immunity in a HeLo-domain-dependent manner

As *Arabidopsis* MLKLs (*At*MLKLs) confer TNL-triggered immunity,[10] we investigated the sub-cellular dynamics of *At*MLKLs during TNL-mediated immunity (Figure 1). We utilized a previously established *Arabidopsis* complementation line expressing *At*MLKL1-GFP under the native *cis*-regulatory sequence in an *Atmlkl1* background[10] and *Nicotiana benthamiana* transiently expressing *At*MLKL1-GFP under a constitutive 35S promoter. We chose *At*MLKL1 for subsequent experiments due to the lower expression of *AtMLKL2* and 3 under native conditions,[10,41] which hinders microscopic examination. We detected a greater number of clustered GFP signals (GFP puncta) in leaf epidermal cells of the *Arabidopsis* line and *N. benthamiana* upon infiltration with *Pseudomonas fluorescens* Pf0-1 (Pf0-1)-expressing bacterial effectors AvrRPS4 and *Xanthomonas* outer protein Q (XopQ) (hereafter Pf0-AvrRPS4 and Pf0-XopQ), respectively (Figures 1B, 1C, and S1A). AvrRPS4 is recognized by the TNL pair RRS1/RPS4 in *Arabidopsis* and XopQ by TNL Roq1 in *N. benthamiana*.[42,43] In addition to the leaf epidermis, *At*MLKL1-GFP formed clusters in leaf mesophyll cells upon expression of AvrRPS4 in protoplasts derived from the *Arabidopsis* complementation line (Figures S1B and S1C). Clustered *At*MLKL1-GFP signals overlapped with fluorescence signals of the PM tracer, FM4-64,[44] in plasmolyzed epidermal cells, indicating that *At*MLKL1 clusters into puncta at the PM (Figure 1D). Furthermore, the localization of *At*MLKL1-GFP signals in the brefeldin A (BFA)-induced vesicle compartment known as the BFA body[45] (Figure S1D), implies that *Arabidopsis* MLKLs are trafficked to and endocytosed from the PM by the Golgi and *trans*-Golgi network/early endosome-mediated secretory pathway.[46] We noted a transient and slight increase of puncta formation upon infiltration with the Pf0-1 strain without effectors (hereafter Pf0-EV) (Figure 1E), suggesting that PAMP-triggered immunity also facilitates *At*MLKL1 puncta formation. *At*MLKL1-GFP accumulation in leaves of the *Arabidopsis* line was comparable at each time point upon infiltration with Pf0-AvrRPS4, Pf0-EV, or mock treatment (Figure 1F). Therefore, altered *At*MLKL protein abundance does not explain induced localization and clustering of *At*MLKL1-GFP at the PM in the TNL-triggered immune response.

Plant MLKL is a multi-domain protein comprising an N-terminal HeLo domain followed by the brace, pseudokinase, and ID regions[10] (Figure 1A). To determine which domain(s) are responsible for *At*MLKL1 oligomerization (potentially explaining induced puncta formation) and/or PM localization, we transiently

(hpi). Right: top-view of leaf epidermal cells of *N. benthamiana* transiently expressing *At*MLKL1-GFP under a 35S promoter upon challenge with Pf0-XopQ or Pf0-EV at 7 hpi.

(C) Quantification of *At*MLKL1-GFP puncta number. Left: puncta number in the *Arabidopsis* complementation line at 5 hpi upon infiltration of Pf0-AvrRPS4 (n = 29) or Pf0-EV (n = 15). Right: puncta number in *N. benthamiana* at 7 hpi upon infiltration of Pf0-XopQ (n = 12) and Pf0-EV (n = 9). Asterisks indicate significant differences at $p < 0.001$.

(D) Clustered *At*MLKL1-GFP signals overlapping with the PM tracer, FM4-64 in the plasmolyzed epidermal cells. The red and blue arrows indicate the PM and cell wall, respectively. White arrowheads indicate the *At*MLKL1-GFP puncta.

(E) A time-course quantification of *At*MLKL1-GFP puncta number in the *Arabidopsis* complementation line.

(F) Steady-state levels of *At*MLKL1-GFP were comparable at each examined time point upon infiltration with Pf0-AvrRPS4, Pf0-EV, and the mock treatment in total cell lysate from the *Arabidopsis* complementation line.

(G) The N-terminal HeLo domain is sufficient and necessary for puncta formation in *N. benthamiana*. No avirulent pathogens were challenged. The images were taken at 48 h after agroinfiltration. White arrowheads indicate the *At*MLKL1-GFP puncta. H, HeLo; H+B, HeLo domain with brace; H+B+P, HeLo domain with brace and pseudokinase; B+P+ID, a variant lacking the HeLo domain.

(H) Disease resistance assay of *At*MLKL1 truncated variants against YFP-expressing PVX in *N. benthamiana*. β-glucuronidase (GUS) derived from *Escherichia coli* was used as a negative control.

(I) Disease resistance assay of the N-terminal HeLo domain of *At*MLKL1 against *Pst* DC3000 in *Atmlkl123* mutant background at 3 dpi. n = 16 from at least three replicates.

See also Figure S1.

Please cite this article in press as: Shen et al., Cytoplasmic calcium influx mediated by plant MLKLs confers TNL-triggered immunity, Cell Host & Microbe (2024), https://doi.org/10.1016/j.chom.2024.02.016

overexpressed a series of C-terminally GFP-tagged *At*MLKL1 truncated variants in *N. benthamiana*, without an ETI trigger (Figure 1G). We found that the HeLo domain alone (H) and the HeLo domain with brace (H+B) variants appeared as puncta at the PM, while neither the HeLo domain with brace and pseudokinase (H+B+P) variant, a variant lacking the HeLo domain (B+P+ID), nor full-length *At*MLKL1 formed puncta (Figure 1G). As the *At*MLKL1 variants were barely detectable upon heterologous expression by immunoblotting (data not shown), we verified their expression by transfecting them into *Arabidopsis* protoplasts, followed by immunoblotting (Figure S1E). Consistent with previous observations,[10] full-length *At*MLKL1 and the H+B+P variants are associated with microtubules (Figures 1G and S1F). Taken together, these results demonstrate that the N-terminal HeLo domain is necessary and sufficient for the puncta formation and the PM localization of *At*MLKL1. They further suggest that the pseudokinase domain is responsible for the autoinhibition of *At*MLKL1.

We next sought to determine which domain(s) of *At*MLK1L are responsible for disease resistance activity. Overexpression of helper NLRs (e.g., NRG1 and ADR1) that contain the HeLo domain at their N terminus conferred resistance against potato virus X (PVX) in the absence of host cell death.[47,48] Therefore, we tested whether *At*MLKL can suppress PVX proliferation by co-expressing HA-tagged *At*MLKL1 or its truncated variants with a PVX variant expressing YFP. Because of a strong positive correlation between PVX-derived YFP signal and PVX RNA (Figure S2A), we measured the YFP intensity of the leaf lysates as a proxy for viral RNA accumulation and, thus, a measure of resistance activity of *At*MLKL1 forms (Figure 1H). The H and H+B variants produced a lower YFP intensity compared with full-length *At*MLKL1 protein, indicating these variants have resistance activity (Figure 1H). By contrast, the H+B+P and B+P+ID variants and the variant lacking the HeLo domain and brace (P+ID) did not limit PVX proliferation (Figure 1H). The HeLo domain also conferred resistance against *Pst* DC3000 in the *Atmlkl123* mutant background (Figure 1I). Taken together, our data suggest that the tetrameric configuration of wild-type *At*MLKLs (Figure 1A), represents an auto-repressed state of this protein family and that *At*MLKLs undergo a drastic conformational change, which exposes the HeLo domains to resistance signaling activity.

*At*MLKL structure-guided mutagenesis reveals an *EDS1*-dependent and RPW8-type helper NLR-independent disease resistance activity

As the disease resistance assay (Figures 1H and 1I) suggests that exposure of the HeLo domains from the tetramer is a pivotal step in plant MLKL activation, we next performed structure-guided mutagenesis in an attempt to disrupt MLKL autorepression. A closer inspection of the *At*MLKL cryo-EM structure identified two intra-domain interactions (Figures 2A and 2B) and one inter-domain interaction (Figures 2C and 2D) that could be a direct cause of the burial of the HeLo domains in the tetramer (Figure 1A). Two intra-domain interactions are mediated by an interface between the HeLo domain and brace region and between the HeLo domain and the pseudokinase, which were named the HB interface and the HP interface, respectively (Figures 2A and 2B), while one inter-domain interaction mediated by an interface between HeLo domains is named the HH interface (Figures 2C and 2D). Among residues involved in the interactions, we substituted the hydrophobic residues with charged glutamate or aspartate. Substitution of these residues is predicted to be thermodynamically unfavorable, destabilizing intra- and inter-domain interactions in the tetramer.

Consistent with our activation model, combinatorial mutation of the HP + HH interfaces resulted in increased disease resistance to PVX compared with the wild-type *At*MLKL1 in *N. benthamiana* (Figure 2E). Similar to the above mutation, mutation in the HP + HB interfaces also resulted in increased resistance (Figure 2E). Compared with the combined mutations, single interface mutations did not increase the disease resistance activity of the respective *At*MLKl1 variants (Figure S2B), suggesting that simultaneous dissociation of these interfaces is required for *At*MLKL1 activation. The previously identified gain-of-function variant carrying a phosphomimetic mutation in the activation loop of the pseudokinase domain[10] also showed increased disease resistance activity (Figure 2E). These gain-of-function variants conferred resistance against PVX without host cell death (Figure S2C). Pathogen-activated TNL receptors recruit EDS1 dimers with RPW8-type helper NLRs (RNLs) of the ADR1 and NRG1 families for downstream signaling.[10,27,28,48,50,51] However, the genetic relationship between RNLs and MLKLs, or between EDS1 and MLKLs, in immunity remains unclear. Therefore, we tested whether the gain-of-function variants of *At*MLKL1 confer immunity in the *adr1 nrg1* knockout mutant[52] or the *eds1 pad4 sag101ab* (*Nb-epss*) mutant of *N. benthamiana*[24] using the PVX-based assay. We found that disease resistance activity of the gain-of function variants was largely retained in an *adr1 nrg1* mutant background, while resistance activity was barely detected in the *Nb-epss* mutant background (Figure 2E). Notably, the N-terminal HeLo domain of human MLKL confers resistance in plants, suggesting the conserved *in vivo* activity of plant and animal MLKLs (Figure S2D). Taken together, our analysis further supports the idea that *At*MLKL tetramers represent an auto-repressed conformation. Moreover, these data imply that RNLs and plant MLKLs can function in a parallel fashion.

The EDS1 circuit is required for *At*MLKL1 clustering during TNL-triggered immunity

As disease resistance activity of *At*MLKL1 is dependent on the EDS1 family in *N. benthamiana* (Figure 2E), we investigated whether *EDS1* is required for the sub-cellular relocalization and oligomerization of *At*MLKL1 during TNL-mediated immunity. For this we transformed the *Arabidopsis eds1-12*[53] mutant with a construct that complements the *Atmlkl1* mutation, restoring endogenous levels of the GFP-tagged *At*MLKL1.[10] Upon infiltration with Pf0-AvrRPS4 triggering TNL immunity, no clustered GFP signals were observed in the *eds1* mutant background in six transgenic lines (Figure 3A), despite comparable steady-state levels of *At*MLKL1-GFP protein in wild-type and *eds1* backgrounds (Figure 3B). In contrast with *At*MLKL1-GFP full-length protein, the GFP-tagged HeLo domain alone clustered around the PM in the *Nb-epss* mutant background (Figure 3C). We attributed this EDS1-independent clustering to autonomous self-association of the *At*MLKL1 HeLo domain as in size-exclusion chromatography, a recombinantly expressed HeLo domain eluted at an estimated molecular weight corresponding to

Please cite this article in press as: Shen et al., Cytoplasmic calcium influx mediated by plant MLKLs confers TNL-triggered immunity, Cell Host & Microbe (2024), https://doi.org/10.1016/j.chom.2024.02.016

CellPress
OPEN ACCESS

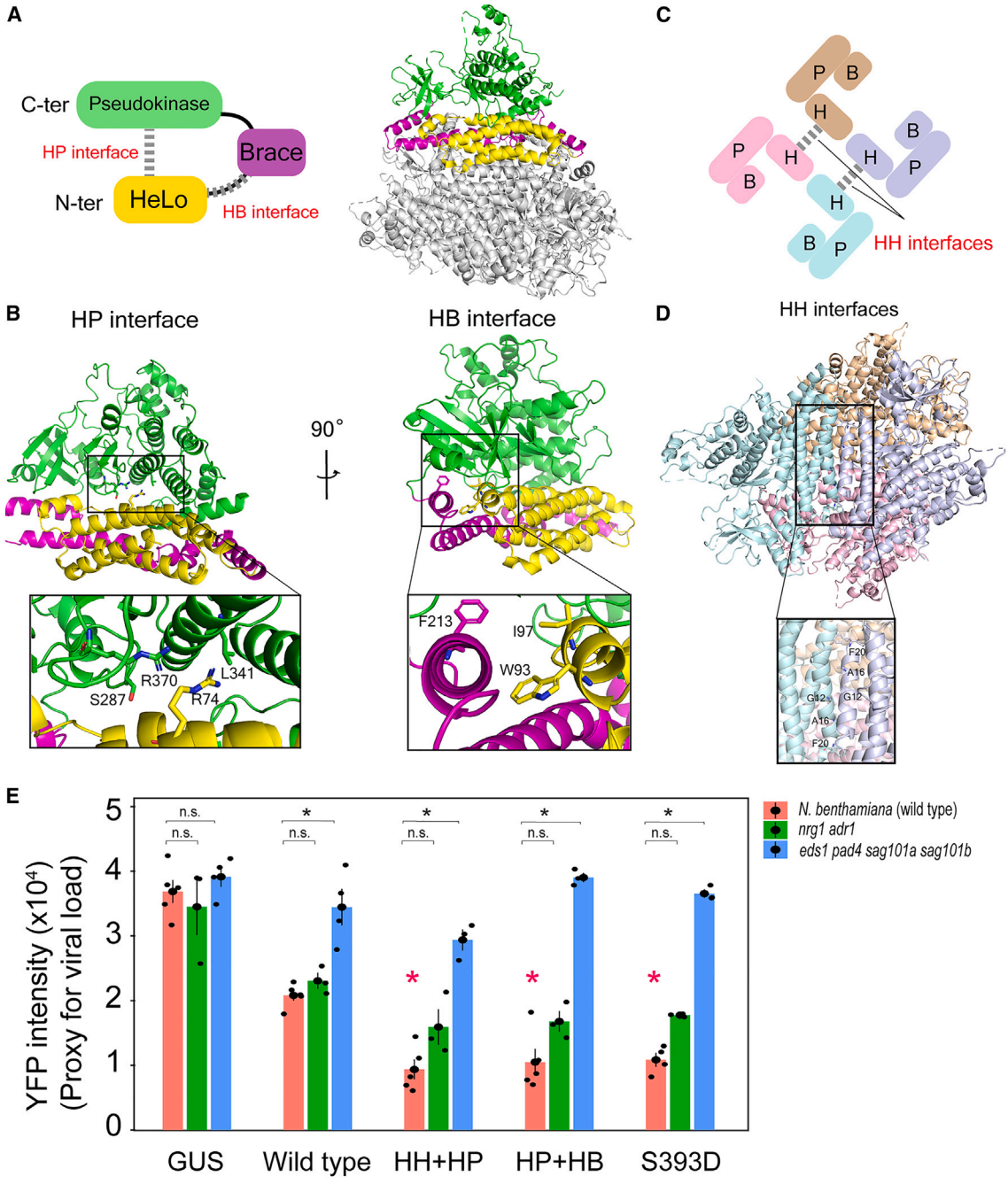

Figure 2. Structure-guided mutagenesis reveals distinct contributions of the EDS1 family and helper NLRs to the disease resistance activity mediated by the gain-of-function variants of *At*MLKL1

(A) Schematic and three-dimensional (3D) structures of *At*MLKLs. Left: schematic representation of the intra-domain interfaces indicated by dashed lines. Right: 3D structure of the *At*MLKL1 tetramer modeled by Alfafold2.[49] As the cryo-EM structures of *At*MLKL2 and *At*MLKL3 are nearly identical, and the protein sequences of *At*MLKL1, 2, and 3 are highly conserved, it is conceivable that *At*MLKL1 also forms an *At*MLKL3-like tetramer. The color code is identical to the left schematic. One of four protomers is shown in color.

(B) The position of amino acid residues in the intra-domain interfaces in the *At*MLKL1 protomer.

(C) Schematic representation of the inter-domain interfaces indicated by dashed lines.

(D) The position of amino acid residues in the inter-domain interfaces in the *At*MLKL1 tetramer.

(E) Disease resistance assay using YFP-expressing PVX. HH+HP and HP+HB indicate *At*MLKL1 variants harboring mutations at the HH+HP interfaces (G12D, A16D, L20D, R74E, S287E, L341E, and R370E) and HP+HB interfaces (R74E, W93A, I97E, F213E, S287E, L341E, and R370E), respectively. The gain-of-function variant S393D[10] served as a positive control. GUS was used as a negative control. The red asterisks indicate significant differences from the wild-type *At*MLKL1 at $p < 0.02$, determined with Dunnett's test. Black asterisks indicate significant differences at $p < 0.01$, which were determined with the Kruskal-Wallis H test. See also Figure S2.

Please cite this article in press as: Shen et al., Cytoplasmic calcium influx mediated by plant MLKLs confers TNL-triggered immunity, Cell Host & Microbe (2024), https://doi.org/10.1016/j.chom.2024.02.016

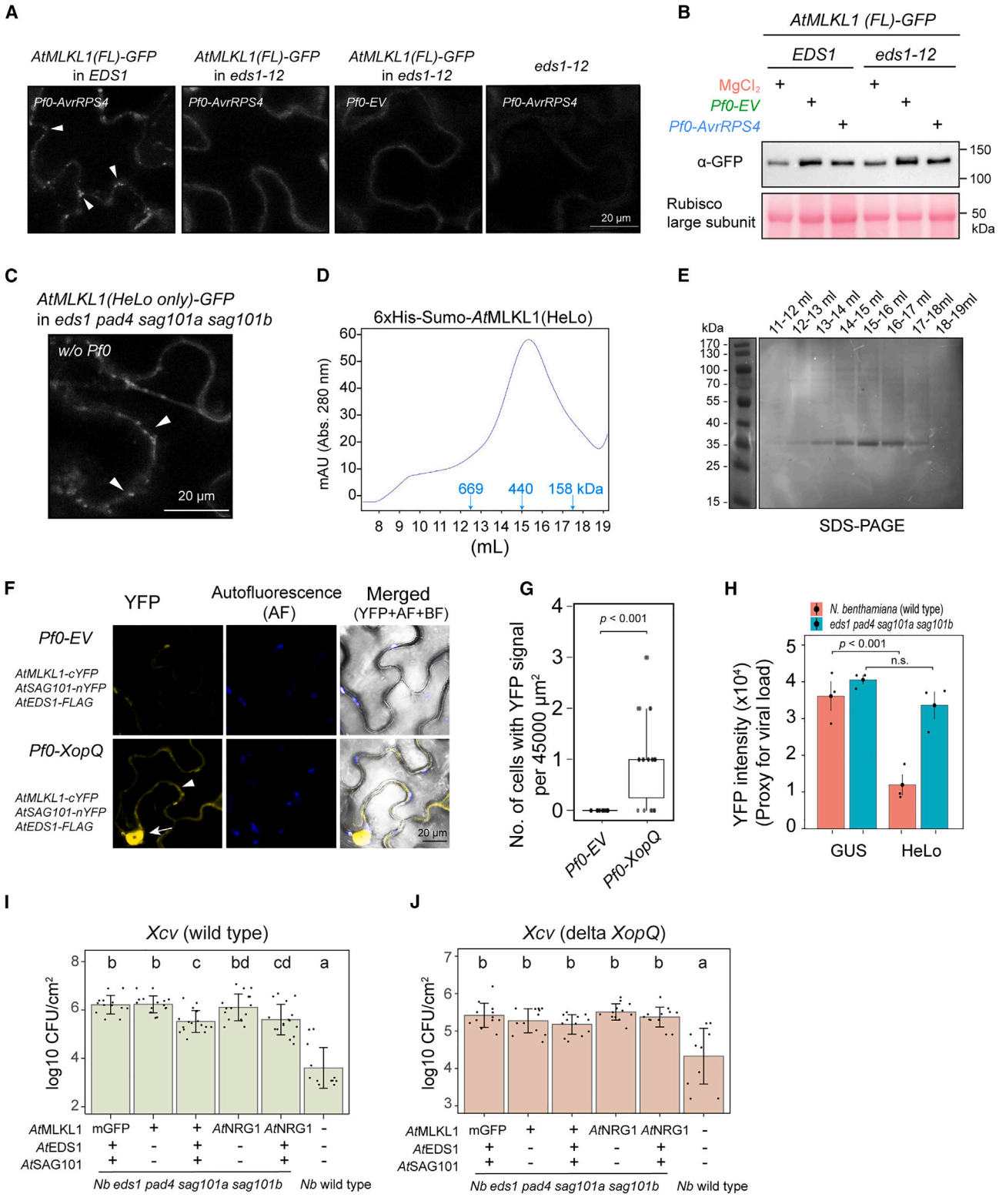

Figure 3. EDS1 facilitates *At*MLKL1 clustering during TNL-triggered immunity

(A) Confocal images of leaf epidermal cells of *Arabidopsis* wild type or *eds1-12* mutant expressing *AtMLKL*1-GFP under the native *cis*-regulatory sequence. White arrowheads indicate the *At*MLKL1-GFP puncta. Images were taken at 5–6 hpi with Pf0-AvrRPS4.

(B) Steady-state levels of *At*MLKL1-GFP in total cell lysate from the indicated *Arabidopsis* lines upon infiltration with Pf0-AvrRPS4, Pf0-EV, and $MgCl_2$. The samples were collected at 5 hpi.

(legend continued on next page)

Please cite this article in press as: Shen et al., Cytoplasmic calcium influx mediated by plant MLKLs confers TNL-triggered immunity, Cell Host & Microbe (2024), https://doi.org/10.1016/j.chom.2024.02.016

approximately 15 protomers (Figures 3D and 3E). These results prompted us to test for interaction between *At*MLKL1 and the *At*EDS1-*At*SAG101 functional dimer in *N. benthamiana* using bimolecular fluorescence complementation (BiFC) and co-immunoprecipitation (coIP) assays. As *Arabidopsis* EDS1 and SAG101 do not co-function with *N. benthamiana* native NRG1,[24] we minimized interference by activated *Nb*NRG1, by transiently co-expressing C-terminally tagged *At*MLKL1, *At*SAG101, and *At*EDS1 in the *Nb-epss* mutant.

A BiFC assay using *At*MLKL1-cYFP, *At*SAG101-nYFP, and *At*EDS1-FLAG constructs detected YFP signals around the PM and at nuclei upon infiltration with Pf0-XopQ, whereas no marked YFP signal was detected upon infiltration with Pf0-EV (Figure 3F). CoIP experiments also supported a *in planta* interaction between *At*SAG101 and *At*MLKL1 (Figures S3B and S3C). Furthermore, co-expression of *At*EDS1, *At*SAG101, and *At*MLKL1 restored some Roq1-mediated resistance to *Xanthomonas campestris pv vesicatoria* that carries XopQ[43] in the *Nb-epss* mutant background (Figure 3I). Unexpectedly, disease resistance-inducing activity of the *At*MLKL1 HeLo domain alone was impaired in *Nb-epss* (Figure 3H). These results suggest that EDS1 and SAG101 not only function in the activation step of *At*MLKL1 but are also involved in signaling downstream of activated *At*MLKLs, which may constitute an immune-amplifying feedback loop (see also discussion).

Plant MLKLs mediate $[Ca^{2+}]_{cyt}$ influx in plant and human cells

Plant MLKLs and RNLs share the N-terminal HeLo four-helix bundle,[10,29,33,34] and the latter was shown to mediate $[Ca^{2+}]_{cyt}$ influx in TNL immunity.[29] Therefore, we examined the role of plant MLKLs in $[Ca^{2+}]_{cyt}$ influx in TNL immunity.[32] Using minimally invasive microscopic analysis, we monitored changes in $[Ca^{2+}]_{cyt}$ in leaves of wild-type and *Atmlkl123* mutant plants expressing the GFP-based Ca^{2+} sensor GCaMP3[54,55] during TNL- or CNL-triggered immune signaling. Unlike wild-type plants, *Atmlk123* mutant plants failed to mount a sustained $[Ca^{2+}]_{cyt}$ increase at 10–14 h post-infiltration with Pf0-AvrRPS4 (Figure 4A), while a transient $[Ca^{2+}]_{cyt}$ increase at around 4 h was detectable in both genotypes (Figure 4A). The transient and sustained $[Ca^{2+}]_{cyt}$ increases were a host response specific to the Pf0-AvrRPS4 strain that activates the TNL pair RRS1/RPS4, as the $[Ca^{2+}]_{cyt}$ increases were undetectable upon infiltration of Pf0-EV (Figure 4A). In agreement with a limited contribution of *At*MLKLs to CNL-triggered immunity,[10] the $[Ca^{2+}]_{cyt}$ increase upon challenge with the Pf0-1 strain expressing AvrRPM1(Pf0-AvrRPM1) that activates the RPM1[56] receptor was similar between wild-type and *Atmlk123* mutant backgrounds (Figure 4B). We noted that in the wild-type plants, the patterns of $[Ca^{2+}]_{cyt}$ influx were markedly different in response to Pf0-AvrRPS4 and Pf0-AvrRPM1 strains, implying distinct impacts of these TNL and CNL receptors on $[Ca^{2+}]_{cyt}$ influx. NRG1.1 and NRG1.2 RNLs are required for full activity of multiple TNLs (e.g., RPP2, RPP4, and RPS4) in *Arabidopsis*.[50] Our analysis did not detect a transient $[Ca^{2+}]_{cyt}$ increase in the leaves of the *nrg1.1,1.2* mutant expressing GCaMP3, whereas an increase in $[Ca^{2+}]_{cyt}$ at 12–14 h post-infiltration was detected (Figure S4A). This increase may result in a delayed but sustained $[Ca^{2+}]_{cyt}$ increase in the *nrg1.1,1.2* mutant. Taken together, our data demonstrate that *At*MLKL1 and the RNLs differentially regulate AvrRPS4-dependent $[Ca^{2+}]_{cyt}$.

As the HeLo domain of *At*MLKL1 is indispensable for both immunity and clustering at the PM (Figure 1), we tested whether the HeLo domains of *At*MLKLs can elicit $[Ca^{2+}]_{cyt}$ influx in human HEK 293 cells. We took advantage of an experimental system that enables chemical (i.e., rapamycin)-induced de-repression of HeLo domain activity (Figures 4E and S4B–S4D). Upon rapamycin treatment, the N-terminal HeLo domain and HeLo domain plus the brace region of *At*MLKL1 induced $[Ca^{2+}]_{cyt}$ influx in human HEK293T cells (Figures 4C and 4D). Notably, the HeLo domain with the brace region of human MLKL (*Hs*MLKL) also elicited $[Ca^{2+}]_{cyt}$ influx in HEK293T cells (Figures 4C and 4D). Whereas the HeLo domain with the brace region of *Hs*MLKL caused necroptotic cell death, neither the HeLo domain of *At*MLKL1 nor the HeLo domain with the brace region of *At*MLKLs caused cell death in HEK293T cells (Figures 4E and S4D). Therefore, plant MLKL-mediated $[Ca^{2+}]_{cyt}$ influx in HEK293T cells is not a consequence of cell death. We detected an induced GCaMP3 signal in stable transgenic *N. benthamiana* plants expressing GCaMP3[57] upon expression of the *At*MLKL1 HeLo domain (Figures 4E and S4F). Taken together, the data suggest that plant MLKLs are recruited by TNL, but not CNL, receptors for signaling leading to pathogen resistance and that plant MLKLs contribute to TNL immunity through HeLo-domain-mediated $[Ca^{2+}]_{cyt}$ influx.

DISCUSSION

We show here that PM-localized plant MLKLs are mediators of $[Ca^{2+}]_{cyt}$ influx. *At*MLKLs are preferentially engaged by TNL- but not CNL-triggered immunity.[10] Consistent with its disease resistance phenotype, the *Atmlkl* null mutant is defective in mediating sustained Ca^{2+} influx during TNL (i.e., RPS4)-triggered immunity and not CNL (i.e., RPM1)-triggered immunity (Figures 4A and 4B). The involvement of plant MLKLs in TNL-triggered immunity is well supported by the observation that an EDS1-SAG101

(C) Confocal images of leaf epidermis of the *Nb-epss* expressing *At*MLKL1(HeLo)-GFP. No avirulent pathogens were challenged. White arrowheads indicate the puncta. The images were taken at 48 h after agroinfiltration.
(D) Size-exclusion chromatography profile of the 6xHis-Sumo-tagged HeLo domain of *At*MLKL1. The position of the molecular weight marker is indicated.
(E) Peak fractions in the size-exclusion chromatography were verified by SDS-PAGE.
(F) BiFC assay between *At*MLKL1 and *At*SAG101 during TNL-triggered immunity. Enhanced YFP signals around the PM and at nuclei are indicated by the white arrowhead and arrow, respectively.
(G) Quantification of the number of cells with YFP signals in BiFC assay upon the infiltration with Pf0-EV (n = 18) or Pf0-XopQ (n = 22).
(H) Disease resistance assay against PVX for the HeLo domain of *At*MLKL1 in the *Nb-epss*.
(I and J) Reconstitution of *At*EDS1-, *At*SAG101-, and *At*MLKL1-mediated immunity in *Nb-epss* against the *X. c. vesicatoria* (*Xcv*) strain. *At*NRG1 served as a positive control.[24] n = 10 to 12 from three independent experiments. Different letters indicate statistically significant differences at $p < 0.05$.
See also Figure S3.

Please cite this article in press as: Shen et al., Cytoplasmic calcium influx mediated by plant MLKLs confers TNL-triggered immunity, Cell Host & Microbe (2024), https://doi.org/10.1016/j.chom.2024.02.016

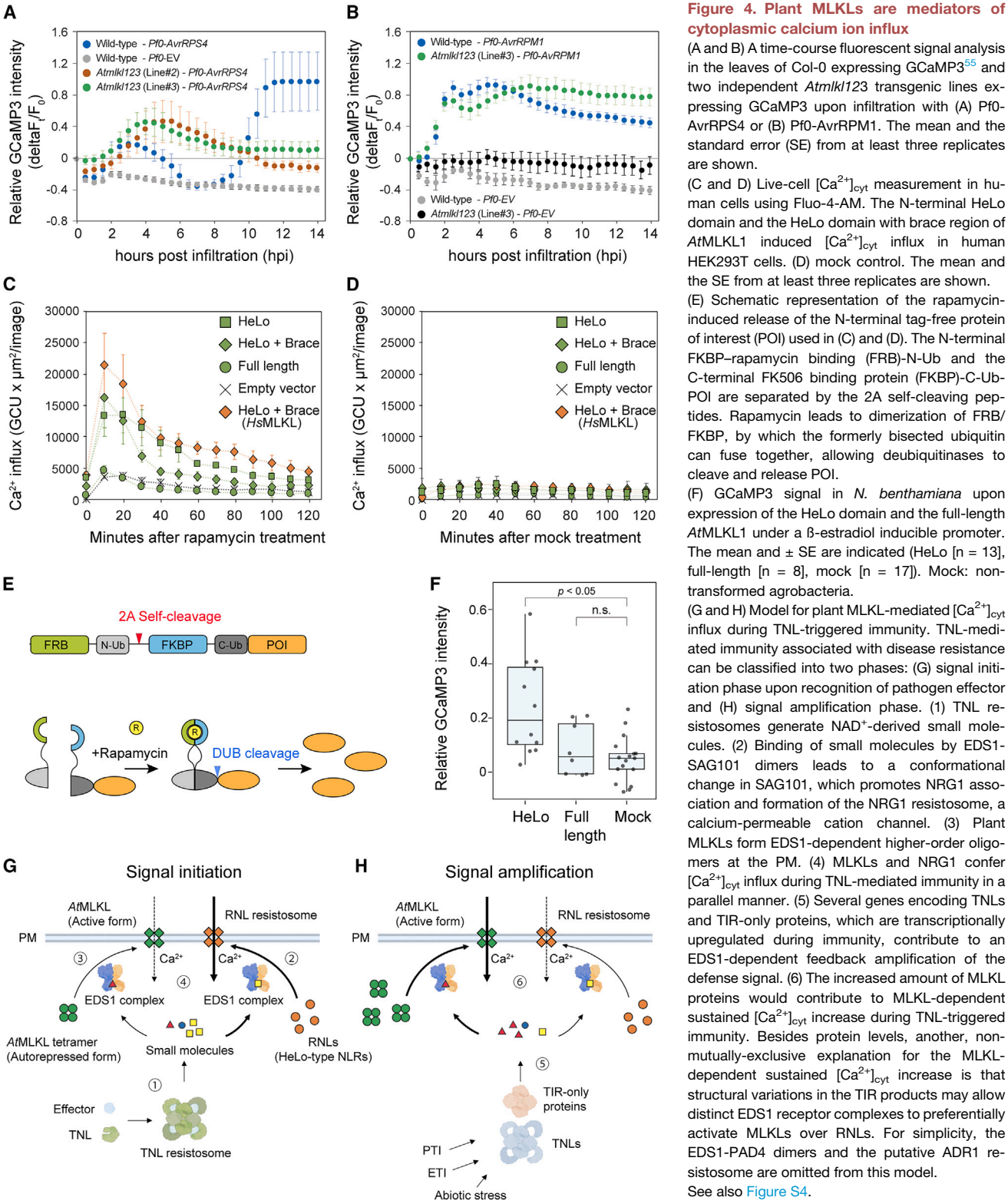

Figure 4. Plant MLKLs are mediators of cytoplasmic calcium ion influx

(A and B) A time-course fluorescent signal analysis in the leaves of Col-0 expressing GCaMP3[55] and two independent *Atmlkl123* transgenic lines expressing GCaMP3 upon infiltration with (A) Pf0-AvrRPS4 or (B) Pf0-AvrRPM1. The mean and the standard error (SE) from at least three replicates are shown.

(C and D) Live-cell $[Ca^{2+}]_{cyt}$ measurement in human cells using Fluo-4-AM. The N-terminal HeLo domain and the HeLo domain with brace region of *At*MLKL1 induced $[Ca^{2+}]_{cyt}$ influx in human HEK293T cells. (D) mock control. The mean and the SE from at least three replicates are shown.

(E) Schematic representation of the rapamycin-induced release of the N-terminal tag-free protein of interest (POI) used in (C) and (D). The N-terminal FKBP–rapamycin binding (FRB)-N-Ub and the C-terminal FK506 binding protein (FKBP)-C-Ub-POI are separated by the 2A self-cleaving peptides. Rapamycin leads to dimerization of FRB/FKBP, by which the formerly bisected ubiquitin can fuse together, allowing deubiquitinases to cleave and release POI.

(F) GCaMP3 signal in *N. benthamiana* upon expression of the HeLo domain and the full-length *At*MLKL1 under a ß-estradiol inducible promoter. The mean and ± SE are indicated (HeLo [n = 13], full-length [n = 8], mock [n = 17]). Mock: non-transformed agrobacteria.

(G and H) Model for plant MLKL-mediated $[Ca^{2+}]_{cyt}$ influx during TNL-triggered immunity. TNL-mediated immunity associated with disease resistance can be classified into two phases: (G) signal initiation phase upon recognition of pathogen effector and (H) signal amplification phase. (1) TNL resistosomes generate NAD^+-derived small molecules. (2) Binding of small molecules by EDS1-SAG101 dimers leads to a conformational change in SAG101, which promotes NRG1 association and formation of the NRG1 resistosome, a calcium-permeable cation channel. (3) Plant MLKLs form EDS1-dependent higher-order oligomers at the PM. (4) MLKLs and NRG1 confer $[Ca^{2+}]_{cyt}$ influx during TNL-mediated immunity in a parallel manner. (5) Several genes encoding TNLs and TIR-only proteins, which are transcriptionally upregulated during immunity, contribute to an EDS1-dependent feedback amplification of the defense signal. (6) The increased amount of MLKL proteins would contribute to MLKL-dependent sustained $[Ca^{2+}]_{cyt}$ increase during TNL-triggered immunity. Besides protein levels, another, non-mutually-exclusive explanation for the MLKL-dependent sustained $[Ca^{2+}]_{cyt}$ increase is that structural variations in the TIR products may allow distinct EDS1 receptor complexes to preferentially activate MLKLs over RNLs. For simplicity, the EDS1-PAD4 dimers and the putative ADR1 resistosome are omitted from this model.

See also Figure S4.

Please cite this article in press as: Shen et al., Cytoplasmic calcium influx mediated by plant MLKLs confers TNL-triggered immunity, Cell Host & Microbe (2024), https://doi.org/10.1016/j.chom.2024.02.016

receptor complex that is targeted by TIR enzyme-generated products is required for *At*MLKL1 clustering at the PM (Figures 3A and 3B). ID proteins can undergo liquid-liquid phase separation (LLPS), a concentration-dependent mechanism responsible for the formation of membrane-free condensates.[58] Although *At*MLKL1 contains an ID region (Figure 1A), the formation of *At*MLKL1 condensates (i.e., puncta) appears to be independent of protein concentration (Figure 1F), and its formation requires EDS1 (Figure 3A). Therefore, it is unlikely that *At*MLKL1 condensates are assembled via LLPS. In animals, the upstream kinase RIPK3 phosphorylates the activation loop of the pseudokinase domain, inducing oligomerization of MLKL monomers.[40,59–62] We envisage that an EDS1 complex might recruit upstream kinase(s) to trigger conformational changes in plant MLKLs, leading to the exposure of its HeLo signaling domains, which possess a propensity for self-oligomerization (Figures 3D and 3E) as well as for triggering Ca^{2+} influx in plant and human cells (Figures 4C–4F).

Consistent with our earlier study,[10] full-length *At*MLKL1 associates with microtubules, and the C-terminal ID region is not required for this association (Figures 1G and S1F). Previous work has shown that BRI1-BIK1 brassinosteroid receptor and FLS2-BIK1 immune receptor complexes are trafficked to distinct PM nanodomains under steady-state conditions, and only the former complex associates with microtubules.[63] Similar to the BRI1-BIK1 complex, *At*MLKL1-GFP localizes to the PM prior to pathogen challenge (Figures S1A and S1D). Therefore, trafficking of *At*MLKL1 via microtubule-related machinery to a specific PM nanodomain may be a prerequisite for clustering of *At*MLKL1 at the PM. In the BiFC assay, *At*MLKL1 associates with *At*SAG101 in nuclei (Figure 3F), despite the absence of a nuclear localization signal in *At*MLKL1. The *Arabidopsis* EDS1-SAG101 dimer has been shown to localize in both the cytoplasm and nucleus.[64,65] Therefore, the stable BiFC complex containing *At*MLKL1 and *At*SAG101, and probably *At*EDS1, can be trafficked to the nucleus, which is facilitated by the EDS1-SAG101 dimer. A similar stable BiFC complex was detected in the nuclei for NRG1 and EDS1-SAG101.[66] As *At*MLKL1-GFP does not localize to the nucleus before or after TNL activation *in A. thaliana* and *N. benthamiana* (Figures 1B and S1A), nuclear localization of *At*MLKL1 may be transient, if it occurs at all.

In necroptosis, oligomerized MLKL permeabilizes the PM via incompletely characterized mechanisms,[67–69] although it is clear that its N-terminal HeLo domain is indispensable.[70,71] Various oligomeric states of activated MLKL have been reported (trimers, tetramers, hexamers, higher-order oligomers, or disulfide-bond-dependent amyloid polymers).[60,62,71–75] The HeLo-domain helices of mouse, human, and plant MLKLs can be classified as amphipathic helices, carrying segregated hydrophilic and hydrophobic surfaces.[8,68] Oligomerization of amphipathic helical proteins is often linked to their activities in membrane lysis.[76–78] In ferroptosis, another type of programmed cell death in animals,[8] partial PM damage results in the formation of a transient pore that causes cytosolic Ca^{2+} influx.[79] A similar mechanism might underlie plant MLKL-mediated cytosolic Ca^{2+} influx. The *Atmlkl*123 mutant exhibits a pronounced sensitivity to filamentous pathogens compared with bacterial pathogens,[10] suggesting that the contribution of plant MLKLs to TNL-triggered immunity varies depending on the mode of pathogen infection.[80,81] Our minimally invasive microscopy-based monitoring of $[Ca^{2+}]_{cyt}$ using GCaMP3 revealed two distinctive AvrRPS4-dependent $[Ca^{2+}]_{cyt}$ increases: a transient $[Ca^{2+}]_{cyt}$ increase and a sustained $[Ca^{2+}]_{cyt}$ increase (Figure 4A). Intriguingly, a transient $[Ca^{2+}]_{cyt}$ increase peaks at 4 h after pathogen challenge in both wild type and the *Atmlkl* null mutant, while the sustained $[Ca^{2+}]_{cyt}$ increase starting at 10 h after pathogen challenge is absent in the *Atmlkl*123mutant (Figure 4A). Instead, a transient $[Ca^{2+}]_{cyt}$ increase is retained in the *Atmlkl123* mutant (Figure 4A), which may partially compensate for the lack of the sustained $[Ca^{2+}]_{cyt}$ increase. Therefore, the defect in sustaining $[Ca^{2+}]_{cyt}$ in *Atmlkl*123 might account for the varying susceptibility of the *Atmlkl* mutant to different types of pathogenic microbes. Additionally, our data suggest that the transient $[Ca^{2+}]_{cyt}$ increase peaking at 4 h is mediated by RNLs (Figure S4A).

Taken together, we propose a model for how two distinct HeLo-domain-containing protein families, namely plant MLKL and RNL, contribute to TNL-mediated immune signaling (Figures 4G and 4H). Recent studies showed that TIR-domain-containing proteins, which are often transcriptionally upregulated during ETI, amplify immune signals at the sites of pathogen infection and/or propagate the signals from the pathogen infection site to distal tissues.[3,4,22,23] Therefore, TNL-mediated immunity can be separated into two phases: (1) a signal initiation phase (Figure 4G) and (2) a signal amplification phase (Figure 4H). We show that *At*MLKLs and RNLs confer TNL-mediated immunity in a parallel manner (Figure 2E). This is also supported by the reconstitution of *Arabidopsis* MLKL-EDS1 signaling in *N. benthamiana* (Figures 3I and 3J). As an *Arabidopsis* EDS1-SAG101 does not substitute for *Nb* EDS1-SAG101, which activates endogenous helper *Nb*NRG1 in *N. benthamiana*,[24] the *At*MLKL1-mediated immunity to *Xcv* expressing XopQ effector in the *Nb-epss* (Figure 3I) is independent of *Nb*NRG1.

Plant MLKLs and RNLs mediate $[Ca^{2+}]_{cyt}$ influx in TNL-mediated immunity (Figures 4A and S4A), but MLKLs contribute to the sustained and intensified $[Ca^{2+}]_{cyt}$ influx (Figure 4A). TIR-derived signal(s) propagation to neighboring cells[22,82] could increase the sum of GCaMP3 fluorescence (thus Ca^{2+} signaling) in certain regions or cell types of the leaf. This might explain why the *Atmlkl*123 mutant is much more susceptible to filamentous pathogens (e.g., powdery mildew), which actively spread from infected cells to neighboring healthy cells, than a leaf-infiltrating bacterial pathogen, (e.g., *P. syringae*), which localizes at the inoculation site within the time frame of an experiment.[10] Increased levels of MLKL proteins (Figure 2F) would contribute to an MLKL-dependent sustained $[Ca^{2+}]_{cyt}$ increase during RPS4-triggered immunity (Figure 4A). Besides MLKL protein elevation, another possibility is that structural variations in TIR-produced metabolites could enable distinctive EDS1 receptor complexes to preferentially activate MLKLs over RNLs. The plant TIR-produced metabolites Phosphoribosyl-AMP (pRib-AMP) and ADP-ribosylated-ATP (ADRr-ATP) promote association of EDS1 receptors with the downstream RNLs NRG1 and ADR1,[27,28] while plant TIR-only proteins like *Bd*TIR generate ~100-fold more 2′ cyclic adenosine diphosphate ribose (2′cADPR), *in planta* relative to TIR domains from TNL proteins.[17,83] Moreover, plant TIR-only proteins are also linked with abiotic stress responses.[84,85] A recent study showed that *At*MLKL1 mediates an abiotic stress response (i.e., salt stress),[86] lending further support to the notion that plant MLKLs are integral signaling components of the TIR pathway.

CellPress
OPEN ACCESS

Cell Host & Microbe
Short article

STAR★METHODS

Detailed methods are provided in the online version of this paper and include the following:

- KEY RESOURCES TABLE
- RESOURCE AVAILABILITY
  - Lead contact
  - Materials availability
  - Data and code availability
- EXPERIMENTAL MODEL AND STUDY PARTICIPANT DETAILS
  - *Arabidopsis thaliana* and growth conditions
  - *Nicotiana benthamiana* and growth conditions
  - Pathogen strains and growth conditions
  - *Agrobacterium tumefaciens* growth condition
  - Human cell and culture conditions
- METHOD DETAILS
  - Ca^{2+} imaging in leaves
  - ß-estradiol-based transient protein expression in *N. benthamiana* for Ca^{2+} imaging
  - Immunoblotting (*N. benthamiana*)
  - Immunoblotting (*A. thaliana*)
  - Pathogen infection assays using YFP-expressing Potato virus X
  - Recombinant protein expression in insect cells and size-exclusion analysis
  - Confocal microscopy
  - Construction of plasmids with *At*MLKL1 variants
  - Transient gene expression in protoplasts
  - Bimolecular fluorescence complementation (BiFC) assays
  - Pathogen infection assays (*Pst* DC3000)
  - *Xanthomonas* growth assay in *N. benthamiana*
  - Drug treatments
  - Immunoprecipitation assays
  - Plasmid construction for protein expression in human cell culture
  - Plasmid transfection into HEK293T cells
  - Immunoblotting (human cells)
  - Live-cell cytoplasmic Ca^{2+} imaging in human cells
  - Cell viability assay in human cells
- QUANTIFICATION AND STATISTICAL ANALYSIS

SUPPLEMENTAL INFORMATION

Supplemental information can be found online at https://doi.org/10.1016/j.chom.2024.02.016.

ACKNOWLEDGMENTS

We thank Uyen Nguyen, Leonie Schroers, and Dennis Mahr for technical assistance and Neysan Donnelly for editing the manuscript. We also thank Frank Takken, Dale Sanders, Keiko Yoshioka, Johannes Stuttmann, Martin Hartmut Schattat, Aaron Lawson, Ulla Bonas for pSfinx plasmid, pBIN20-35s-GCaMP3 plasmid/GCaMP3 *Arabidopsis* line, GCaMP3 *Nicotiana* line, *Nbeds1*, *Nbadr1nrg1* mutant, CMV2b/P19 plasmids, and *Xcv* 85-10 strain, respectively. We thank Paul Schulze-Lefert and the Max Planck Society for generously allowing Q.S., K. Hasegawa, A.P., L.W.T., and T.M. access to laboratory equipment, which was particularly helpful during the COVID-19 pandemic. This work was supported by the Deutsche Forschungsgemeinschaft (DFG, German Research Foundation, SFB-1403–414786233 to K. Hofmann, J.E.P., J.C., and T.M.), a grant from the University of Cologne Centre of Excellence in Plant Sciences (T.M.), and the Alexander Von Humboldt Foundation (a Humboldt professorship to J.C.). A part of Figure 4 was prepared with BioRender.com.

AUTHOR CONTRIBUTIONS

J.C. and T.M. conceptualized the project; Q.S., K. Hasegawa, N.O., A.P., L.W.T., J.W., F.R., A.T., J.W., and J.C.C. performed experiments; Q.S., K. Hasegawa, N.O., A.P., L.W.T., J.W., F.R., A.T., J.C.C., K. Hofmann, J.E.P., J.C., and T.M. validated the data; T.T., K. Hofmann, J.E.P., J.C., and T.M. supervised the work; Q.S., K. Hasegawa, and T.M. wrote the paper, with co-author contributions. The first two authors should be regarded as joint first authors. Co-first authors can prioritize their names when adding this paper's references to their resumes.

DECLARATION OF INTERESTS

The authors declare no competing interests.

Received: September 18, 2023
Revised: January 29, 2024
Accepted: February 28, 2024
Published: March 20, 2024

REFERENCES

1. Ngou, B.P.M., Ahn, H.-K., Ding, P., and Jones, J.D.G. (2021). Mutual potentiation of plant immunity by cell-surface and intracellular receptors. Nature *592*, 110–115.
2. Yuan, M., Ngou, B.P.M., Ding, P., and Xin, X.F. (2021). PTI-ETI crosstalk: an integrative view of plant immunity. Curr. Opin. Plant Biol. *62*, 102030.
3. Tian, H., Wu, Z., Chen, S., Ao, K., Huang, W., Yaghmaiean, H., Sun, T., Xu, F., Zhang, Y., Wang, S., et al. (2021). Activation of TIR signalling boosts pattern-triggered immunity. Nature *598*, 500–503.
4. Pruitt, R.N., Locci, F., Wanke, F., Zhang, L., Saile, S.C., Joe, A., Karelina, D., Hua, C., Fröhlich, K., Wan, W.-L., et al. (2021). The EDS1–PAD4–ADR1 node mediates Arabidopsis pattern-triggered immunity. Nature *598*, 495–499.
5. Contreras, M.P., Lüdke, D., Pai, H., Toghani, A., and Kamoun, S. (2023). NLR receptors in plant immunity: making sense of the alphabet soup. EMBO Rep. *24*, e57495.
6. Yuan, M., Cai, B., and Xin, X.-F. (2023). Plant immune receptor pathways as a united front against pathogens. PLoS Pathog. *19*, e1011106.
7. Jacob, F., Vernaldi, S., and Maekawa, T. (2013). Evolution and Conservation of Plant NLR Functions. Front. Immunol. *4*, 297.
8. Maekawa, T., Kashkar, H., and Coll, N.S. (2023). Dying in self-defence: a comparative overview of immunogenic cell death signalling in animals and plants. Cell Death Differ. *30*, 258–268.
9. Jubic, L.M., Saile, S., Furzer, O.J., El Kasmi, F., and Dangl, J.L. (2019). Help wanted: helper NLRs and plant immune responses. Curr. Opin. Plant Biol. *50*, 82–94.
10. Mahdi, L.K., Huang, M., Zhang, X., Nakano, R.T., Kopp, L.B., Saur, I.M.L., Jacob, F., Kovacova, V., Lapin, D., Parker, J.E., et al. (2020). Discovery of a Family of Mixed Lineage Kinase Domain-like Proteins in Plants and Their Role in Innate Immune Signaling. Cell Host Microbe *28*, 813–824.e6.
11. Wang, J., Hu, M., Wang, J., Qi, J., Han, Z., Wang, G., Qi, Y., Wang, H.-W., Zhou, J.-M., and Chai, J. (2019). Reconstitution and structure of a plant NLR resistosome conferring immunity. Science *364*, eaav5870.
12. Davis, B.K., Wen, H., and Ting, J.P. (2011). The inflammasome NLRs in immunity, inflammation, and associated diseases. Annu. Rev. Immunol. *29*, 707–735.
13. Ma, S., Lapin, D., Liu, L., Sun, Y., Song, W., Zhang, X., Logemann, E., Yu, D., Wang, J., Jirschitzka, J., et al. (2020). Direct pathogen-induced

assembly of an NLR immune receptor complex to form a holoenzyme. Science *370*, eabe3069.

14. Martin, R., Qi, T., Zhang, H., Liu, F., King, M., Toth, C., Nogales, E., and Staskawicz, B.J. (2020). Structure of the activated ROQ1 resistosome directly recognizing the pathogen effector XopQ. Science *370*, eabd9993.
15. Li, L., Habring, A., Wang, K., and Weigel, D. (2020). Atypical Resistance Protein RPW8/HR Triggers Oligomerization of the NLR Immune Receptor RPP7 and Autoimmunity. Cell Host Microbe *27*, 405–417.e6.
16. Bi, G., Su, M., Li, N., Liang, Y., Dang, S., Xu, J., Hu, M., Wang, J., Zou, M., Deng, Y., et al. (2021). The ZAR1 resistosome is a calcium-permeable channel triggering plant immune signaling. Cell *184*, 3528–3541.e12.
17. Wan, L., Essuman, K., Anderson, R.G., Sasaki, Y., Monteiro, F., Chung, E.-H., Osborne Nishimura, E., DiAntonio, A., Milbrandt, J., Dangl, J.L., and Nishimura, M.T. (2019). TIR domains of plant immune receptors are NAD^+-cleaving enzymes that promote cell death. Science *365*, 799–803.
18. Nishimura, M.T., Anderson, R.G., Cherkis, K.A., Law, T.F., Liu, Q.L., Machius, M., Nimchuk, Z.L., Yang, L., Chung, E.-H., El Kasmi, F., et al. (2017). TIR-only protein RBA1 recognizes a pathogen effector to regulate cell death in *Arabidopsis*. Proc. Natl. Acad. Sci. USA *114*, E2053–E2062.
19. Essuman, K., Milbrandt, J., Dangl, J.L., and Nishimura, M.T. (2022). Shared TIR enzymatic functions regulate cell death and immunity across the tree of life. Science *377*, eabo0001.
20. Bayless, A.M., Chen, S., Ogden, S.C., Xu, X., Sidda, J.D., Manik, M.K., Li, S., Kobe, B., Ve, T., Song, L., et al. (2023). Plant and prokaryotic TIR domains generate distinct cyclic ADPR NADase products. Sci. Adv. *9*, eade8487.
21. Horsefield, S., Burdett, H., Zhang, X., Manik, M.K., Shi, Y., Chen, J., Qi, T., Gilley, J., Lai, J.S., Rank, M.X., et al. (2019). NAD^+ cleavage activity by animal and plant TIR domains in cell death pathways. Science *365*, 793–799.
22. Jacob, P., Hige, J., Song, L., Bayless, A., Russ, D., Bonardi, V., El Kasmi, F., Wünsch, L., Yang, Y., Fitzpatrick, C.R., et al. (2023). Broader functions of TIR domains in Arabidopsis immunity. Proc. Natl. Acad. Sci. USA *120*, e2220921120.
23. Johanndrees, O., Baggs, E.L., Uhlmann, C., Locci, F., Läßle, H.L., Melkonian, K., Käufer, K., Dongus, J.A., Nakagami, H., Krasileva, K.V., et al. (2023). Variation in plant Toll/Interleukin-1 receptor domain protein dependence on ENHANCED DISEASE SUSCEPTIBILITY 1. Plant Physiol. *191*, 626–642.
24. Lapin, D., Kovacova, V., Sun, X., Dongus, J.A., Bhandari, D., von Born, P., Bautor, J., Guarneri, N., Rzemieniewski, J., Stuttmann, J., et al. (2019). A Coevolved EDS1-SAG101-NRG1 Module Mediates Cell Death Signaling by TIR-Domain Immune Receptors. Plant Cell *31*, 2430–2455.
25. Qi, T., Seong, K., Thomazella, D.P.T., Kim, J.R., Pham, J., Seo, E., Cho, M.-J., Schultink, A., and Staskawicz, B.J. (2018). NRG1 functions downstream of EDS1 to regulate TIR-NLR-mediated plant immunity in *Nicotiana benthamiana*. Proc. Natl. Acad. Sci. USA *115*, E10979–E10987.
26. Sun, X., Lapin, D., Feehan, J.M., Stolze, S.C., Kramer, K., Dongus, J.A., Rzemieniewski, J., Blanvillain-Baufumé, S., Harzen, A., Bautor, J., et al. (2021). Pathogen effector recognition-dependent association of NRG1 with EDS1 and SAG101 in TNL receptor immunity. Nat. Commun. *12*, 3335.
27. Huang, S., Jia, A., Song, W., Hessler, G., Meng, Y., Sun, Y., Xu, L., Laessle, H., Jirschitzka, J., Ma, S., et al. (2022). Identification and receptor mechanism of TIR-catalyzed small molecules in plant immunity. Science *377*, eabq3297.
28. Jia, A., Huang, S., Song, W., Wang, J., Meng, Y., Sun, Y., Xu, L., Laessle, H., Jirschitzka, J., Hou, J., et al. (2022). TIR-catalyzed ADP-ribosylation reactions produce signaling molecules for plant immunity. Science *377*, eabq8180.
29. Jacob, P., Kim, N.H., Wu, F., El-Kasmi, F., Chi, Y., Walton, W.G., Furzer, O.J., Lietzan, A.D., Sunil, S., Kempthorn, K., et al. (2021). Plant "helper" immune receptors are Ca2+-permeable nonselective cation channels. Science *373*, 420–425.
30. Saile, S.C., Ackermann, F.M., Sunil, S., Keicher, J., Bayless, A., Bonardi, V., Wan, L., Doumane, M., Stöbbe, E., Jaillais, Y., et al. (2021). Arabidopsis ADR1 helper NLR immune receptors localize and function at the plasma membrane in a phospholipid dependent manner. New Phytol. *232*, 2440–2456.
31. Wang, Z., Liu, X., Yu, J., Yin, S., Cai, W., Kim, N.H., El Kasmi, F., Dangl, J.L., and Wan, L. (2023). Plasma membrane association and resistosome formation of plant helper immune receptors. Proc. Natl. Acad. Sci. USA *120*, e2222036120.
32. Grant, M., Brown, I., Adams, S., Knight, M., Ainslie, A., and Mansfield, J. (2000). The RPM1 plant disease resistance gene facilitates a rapid and sustained increase in cytosolic calcium that is necessary for the oxidative burst and hypersensitive cell death. Plant J. *23*, 441–450.
33. Fedorova, N.D., Badger, J.H., Robson, G.D., Wortman, J.R., and Nierman, W.C. (2005). Comparative analysis of programmed cell death pathways in filamentous fungi. BMC Genomics *6*, 177.
34. Maruta, N., Burdett, H., Lim, B.Y.J., Hu, X., Desa, S., Manik, M.K., and Kobe, B. (2022). Structural basis of NLR activation and innate immune signalling in plants. Immunogenetics *74*, 5–26.
35. Burdett, H., Bentham, A.R., Williams, S.J., Dodds, P.N., Anderson, P.A., Banfield, M.J., and Kobe, B. (2019). The Plant "Resistosome": Structural Insights into Immune Signaling. Cell Host Microbe *26*, 193–201.
36. Daskalov, A. (2023). Emergence of the fungal immune system. iScience *26*, 106793.
37. Saupe, S.J. (2011). The [Het-s] prion of Podospora anserina and its role in heterokaryon incompatibility. Semin. Cell Dev. Biol. *22*, 460–468.
38. Wang, G., Zhang, D., Orchard, R.C., Hancks, D.C., and Reese, T.A. (2023). Norovirus MLKL-like protein initiates cell death to induce viral egress. Nature *616*, 152–158.
39. Murphy, J.M., Czabotar, P.E., Hildebrand, J.M., Lucet, I.S., Zhang, J.G., Alvarez-Diaz, S., Lewis, R., Lalaoui, N., Metcalf, D., Webb, A.I., et al. (2013). The pseudokinase MLKL mediates necroptosis via a molecular switch mechanism. Immunity *39*, 443–453.
40. Sun, L., Wang, H., Wang, Z., He, S., Chen, S., Liao, D., Wang, L., Yan, J., Liu, W., Lei, X., and Wang, X. (2012). Mixed lineage kinase domain-like protein mediates necrosis signaling downstream of RIP3 kinase. Cell *148*, 213–227.
41. Jacob, F., Kracher, B., Mine, A., Seyfferth, C., Blanvillain-Baufumé, S., Parker, J.E., Tsuda, K., Schulze-Lefert, P., and Maekawa, T. (2018). A dominant-interfering camta3 mutation compromises primary transcriptional outputs mediated by both cell surface and intracellular immune receptors in Arabidopsis thaliana. New Phytol. *217*, 1667–1680.
42. Saucet, S.B., Ma, Y., Sarris, P.F., Furzer, O.J., Sohn, K.H., and Jones, J.D.G. (2015). Two linked pairs of Arabidopsis TNL resistance genes independently confer recognition of bacterial effector AvrRps4. Nat. Commun. *6*, 6338.
43. Schultink, A., Qi, T., Lee, A., Steinbrenner, A.D., and Staskawicz, B. (2017). Roq1 mediates recognition of the Xanthomonas and Pseudomonas effector proteins XopQ and HopQ1. Plant J. *92*, 787–795.
44. Rigal, A., Doyle, S.M., and Robert, S. (2015). Live cell imaging of FM4-64, a tool for tracing the endocytic pathways in Arabidopsis root cells. Methods Mol. Biol. *1242*, 93–103.
45. Orci, L., Perrelet, A., Ravazzola, M., Wieland, F.T., Schekman, R., and Rothman, J.E. (1993). "BFA bodies": a subcompartment of the endoplasmic reticulum. Proc. Natl. Acad. Sci. USA *90*, 11089–11093.
46. Ponnambalam, S., and Baldwin, S.A. (2003). Constitutive protein secretion from the trans-Golgi network to the plasma membrane. Mol. Membr. Biol. *20*, 129–139.
47. Peart, J.R., Mestre, P., Lu, R., Malcuit, I., and Baulcombe, D.C. (2005). NRG1, a CC-NB-LRR Protein, together with N, a TIR-NB-LRR Protein,

Mediates Resistance against Tobacco Mosaic Virus. Curr. Biol. *15*, 968–973.

48. Collier, S.M., Hamel, L.-P., and Moffett, P. (2011). Cell Death Mediated by the N-Terminal Domains of a Unique and Highly Conserved Class of NB-LRR Protein. Mol. Plant. Microbe Interact. *24*, 918–931.
49. Jumper, J., Evans, R., Pritzel, A., Green, T., Figurnov, M., Ronneberger, O., Tunyasuvunakool, K., Bates, R., Žídek, A., Potapenko, A., et al. (2021). Highly accurate protein structure prediction with AlphaFold. Nature *596*, 583–589.
50. Castel, B., Ngou, P.-M., Cevik, V., Redkar, A., Kim, D.-S., Yang, Y., Ding, P., and Jones, J.D.G. (2019). Diverse NLR immune receptors activate defence via the RPW8-NLR NRG1. New Phytol. *222*, 966–980.
51. Gong, Y., Tian, L., Kontos, I., Li, J., and Li, X. (2023). Plant immune signaling network mediated by helper NLRs. Curr. Opin. Plant Biol. *73*, 102354.
52. Prautsch, J., Erickson, J.L., Özyürek, S., Gormanns, R., Franke, L., Lu, Y., Marx, J., Niemeyer, F., Parker, J.E., Stuttmann, J., and Schattat, M.H. (2023). Effector XopQ-induced stromule formation in Nicotiana benthamiana depends on ETI signaling components ADR1 and NRG1. Plant Physiol. *191*, 161–176.
53. Ordon, J., Gantner, J., Kemna, J., Schwalgun, L., Reschke, M., Streubel, J., Boch, J., and Stuttmann, J. (2017). Generation of chromosomal deletions in dicotyledonous plants employing a user-friendly genome editing toolkit. Plant J. *89*, 155–168.
54. Tian, L., Hires, S.A., Mao, T., Huber, D., Chiappe, M.E., Chalasani, S.H., Petreanu, L., Akerboom, J., McKinney, S.A., Schreiter, E.R., et al. (2009). Imaging neural activity in worms, flies and mice with improved GCaMP calcium indicators. Nat. Methods *6*, 875–881.
55. Vincent, T.R., Avramova, M., Canham, J., Higgins, P., Bilkey, N., Mugford, S.T., Pitino, M., Toyota, M., Gilroy, S., Miller, A.J., et al. (2017). Interplay of Plasma Membrane and Vacuolar Ion Channels, Together with BAK1, Elicits Rapid Cytosolic Calcium Elevations in Arabidopsis during Aphid Feeding. Plant Cell *29*, 1460–1479.
56. Grant, M.R., Godiard, L., Straube, E., Ashfield, T., Lewald, J., Sattler, A., Innes, R.W., and Dangl, J.L. (1995). Structure of the Arabidopsis RPM1 Gene Enabling Dual Specificity Disease Resistance. Science *269*, 843–846.
57. DeFalco, T.A., Toyota, M., Phan, V., Karia, P., Moeder, W., Gilroy, S., and Yoshioka, K. (2017). Using GCaMP3 to Study Ca2+ Signaling in Nicotiana Species. Plant Cell Physiol. *58*, 1173–1184.
58. Alberti, S., Gladfelter, A., and Mittag, T. (2019). Considerations and Challenges in Studying Liquid-Liquid Phase Separation and Biomolecular Condensates. Cell *176*, 419–434.
59. Wang, H., Sun, L., Su, L., Rizo, J., Liu, L., Wang, L.F., Wang, F.S., and Wang, X. (2014). Mixed lineage kinase domain-like protein MLKL causes necrotic membrane disruption upon phosphorylation by RIP3. Mol. Cell *54*, 133–146.
60. Liu, S., Liu, H., Johnston, A., Hanna-Addams, S., Reynoso, E., Xiang, Y., and Wang, Z. (2017). MLKL forms disulfide bond-dependent amyloid-like polymers to induce necroptosis. Proc. Natl. Acad. Sci. USA *114*, E7450–E7459.
61. Garnish, S.E., Meng, Y., Koide, A., Sandow, J.J., Denbaum, E., Jacobsen, A.V., Yeung, W., Samson, A.L., Horne, C.R., Fitzgibbon, C., et al. (2021). Conformational interconversion of MLKL and disengagement from RIPK3 precede cell death by necroptosis. Nat. Commun. *12*, 2211.
62. Petrie, E.J., Sandow, J.J., Jacobsen, A.V., Smith, B.J., Griffin, M.D.W., Lucet, I.S., Dai, W., Young, S.N., Tanzer, M.C., Wardak, A., et al. (2018). Conformational switching of the pseudokinase domain promotes human MLKL tetramerization and cell death by necroptosis. Nat. Commun. *9*, 2422.
63. Bücherl, C.A., Jarsch, I.K., Schudoma, C., Segonzac, C., Mbengue, M., Robatzek, S., MacLean, D., Ott, T., and Zipfel, C. (2017). Plant immune and growth receptors share common signalling components but localise to distinct plasma membrane nanodomains. eLife *6*, e25114.
64. García, A.V., Blanvillain-Baufumé, S., Huibers, R.P., Wiermer, M., Li, G., Gobbato, E., Rietz, S., and Parker, J.E. (2010). Balanced nuclear and cytoplasmic activities of EDS1 are required for a complete plant innate immune response. PLoS Pathog. *6*, e1000970.
65. Feys, B.J., Wiermer, M., Bhat, R.A., Moisan, L.J., Medina-Escobar, N., Neu, C., Cabral, A., and Parker, J.E. (2005). Arabidopsis SENESCENCE-ASSOCIATED GENE101 stabilizes and signals within an ENHANCED DISEASE SUSCEPTIBILITY1 complex in plant innate immunity. Plant Cell *17*, 2601–2613.
66. Feehan, J.M., Wang, J., Sun, X., Choi, J., Ahn, H.-K., Ngou, B.P.M., Parker, J.E., and Jones, J.D.G. (2023). Oligomerization of a plant helper NLR requires cell-surface and intracellular immune receptor activation. Proc. Natl. Acad. Sci. USA *120*, e2210406120.
67. Grootjans, S., Vanden Berghe, T., and Vandenabeele, P. (2017). Initiation and execution mechanisms of necroptosis: an overview. Cell Death Differ. *24*, 1184–1195.
68. Flores-Romero, H., Ros, U., and Garcia-Saez, A.J. (2020). Pore formation in regulated cell death. EMBO J. *39*, e105753.
69. Bi, G., and Zhou, J.M. (2021). Regulation of Cell Death and Signaling by Pore-Forming Resistosomes. Annu. Rev. Phytopathol. *59*, 239–263.
70. Su, L., Quade, B., Wang, H., Sun, L., Wang, X., and Rizo, J. (2014). A plug release mechanism for membrane permeation by MLKL. Structure *22*, 1489–1500.
71. Hildebrand, J.M., Tanzer, M.C., Lucet, I.S., Young, S.N., Spall, S.K., Sharma, P., Pierotti, C., Garnier, J.-M., Dobson, R.C.J., Webb, A.I., et al. (2014). Activation of the pseudokinase MLKL unleashes the four-helix bundle domain to induce membrane localization and necroptotic cell death. Proc. Natl. Acad. Sci. USA *111*, 15072–15077.
72. Chen, X., Li, W., Ren, J., Huang, D., He, W.T., Song, Y., Yang, C., Li, W., Zheng, X., Chen, P., and Han, J. (2014). Translocation of mixed lineage kinase domain-like protein to plasma membrane leads to necrotic cell death. Cell Res. *24*, 105–121.
73. Cai, Z., Jitkaew, S., Zhao, J., Chiang, H.C., Choksi, S., Liu, J., Ward, Y., Wu, L.G., and Liu, Z.G. (2014). Plasma membrane translocation of trimerized MLKL protein is required for TNF-induced necroptosis. Nat. Cell Biol. *16*, 55–65.
74. Huang, D., Zheng, X., Wang, Z.A., Chen, X., He, W.T., Zhang, Y., Xu, J.G., Zhao, H., Shi, W., Wang, X., et al. (2017). The MLKL Channel in Necroptosis Is an Octamer Formed by Tetramers in a Dyadic Process. Mol. Cell. Biol. *37*. e00497–16.
75. Davies, K.A., Tanzer, M.C., Griffin, M.D.W., Mok, Y.F., Young, S.N., Qin, R., Petrie, E.J., Czabotar, P.E., Silke, J., and Murphy, J.M. (2018). The brace helices of MLKL mediate interdomain communication and oligomerisation to regulate cell death by necroptosis. Cell Death Differ. *25*, 1567–1580.
76. Tayeb-Fligelman, E., Tabachnikov, O., Moshe, A., Goldshmidt-Tran, O., Sawaya, M.R., Coquelle, N., Colletier, J.P., and Landau, M. (2017). The cytotoxic Staphylococcus aureus PSMα3 reveals a cross-α amyloid-like fibril. Science *355*, 831–833.
77. Adachi, H., Kamoun, S., and Maqbool, A. (2019). A resistosome-activated 'death switch'. Nat. Plants *5*, 457–458.
78. Kayagaki, N., Stowe, I.B., Alegre, K., Deshpande, I., Wu, S., Lin, Z., Kornfeld, O.S., Lee, B.L., Zhang, J., Liu, J., et al. (2023). Inhibiting membrane rupture with NINJ1 antibodies limits tissue injury. Nature *618*, 1072–1077.
79. Pedrera, L., Espiritu, R.A., Ros, U., Weber, J., Schmitt, A., Stroh, J., Hailfinger, S., von Karstedt, S., and García-Sáez, A.J. (2021). Ferroptotic pores induce Ca2+ fluxes and ESCRT-III activation to modulate cell death kinetics. Cell Death Differ. *28*, 1644–1657.
80. Antonovics, J. (1994). The Interplay of Numerical and Gene-Frequency Dynamics tin Host-Pathogen Systems. In Ecological Genetics, R. Leslie, ed. (Princeton University Press), pp. 129–145.

81. Real, L.A., and McElhany, P. (1996). Spatial Pattern and Process in Plant–Pathogen Interactions. Ecology *77*, 1011–1025.

82. Jacob, P., Hige, J., and Dangl, J.L. (2023). Is localized acquired resistance the mechanism for effector-triggered disease resistance in plants? Nat. Plants *9*, 1184–1190.

83. Manik, M.K., Shi, Y., Li, S., Zaydman, M.A., Damaraju, N., Eastman, S., Smith, T.G., Gu, W., Masic, V., Mosaiab, T., et al. (2022). Cyclic ADP ribose isomers: Production, chemical structures, and immune signaling. Science *377*, eadc8969.

84. Kosmacz, M., Luzarowski, M., Kerber, O., Leniak, E., Gutiérrez-Beltrán, E., Moreno, J.C., Gorka, M., Szlachetko, J., Veyel, D., Graf, A., and Skirycz, A. (2018). Interaction of 2′,3′-cAMP with Rbp47b Plays a Role in Stress Granule Formation. Plant Physiol. *177*, 411–421.

85. Yu, D., Song, W., Tan, E.Y.J., Liu, L., Cao, Y., Jirschitzka, J., Li, E., Logemann, E., Xu, C., Huang, S., et al. (2022). TIR domains of plant immune receptors are 2′,3′-cAMP/cGMP synthetases mediating cell death. Cell *185*, 2370–2386.e18.

86. Awlia, M., Alshareef, N., Saber, N., Korte, A., Oakey, H., Panzarová, K., Trtílek, M., Negrão, S., Tester, M., and Julkowska, M.M. (2021). Genetic mapping of the early responses to salt stress in Arabidopsis thaliana. Plant J. *107*, 544–563.

87. Thieme, F., Koebnik, R., Bekel, T., Berger, C., Boch, J., Büttner, D., Caldana, C., Gaigalat, L., Goesmann, A., Kay, S., et al. (2005). Insights into genome plasticity and pathogenicity of the plant pathogenic bacterium Xanthomonas campestris pv. vesicatoria revealed by the complete genome sequence. J. Bacteriol. *187*, 7254–7266.

88. Xing, Y., Xu, N., Bhandari, D.D., Lapin, D., Sun, X., Luo, X., Wang, Y., Cao, J., Wang, H., Coaker, G., et al. (2021). Bacterial effector targeting of a plant iron sensor facilitates iron acquisition and pathogen colonization. Plant Cell *33*, 2015–2031.

89. Schindelin, J., Arganda-Carreras, I., Frise, E., Kaynig, V., Longair, M., Pietzsch, T., Preibisch, S., Rueden, C., Saalfeld, S., Schmid, B., et al. (2012). Fiji: an open-source platform for biological-image analysis. Nat. Methods *9*, 676–682.

90. Clough, S.J., and Bent, A.F. (1998). Floral dip: a simplified method for Agrobacterium-mediated transformation of Arabidopsis thaliana. Plant J. *16*, 735–743.

91. Koncz, C., and Schell, J. (1986). The promoter of TL-DNA gene 5 controls the tissue-specific expression of chimaeric genes carried by a novel type of Agrobacterium binary vector. Mol. Gen. Genet. MGG *204*, 383–396.

92. Ma, L., Lukasik, E., Gawehns, F., and Takken, F.L. (2012). The use of agroinfiltration for transient expression of plant resistance and fungal effector proteins in Nicotiana benthamiana leaves. Methods Mol. Biol. *835*, 61–74.

93. Curtis, M.D., and Grossniklaus, U. (2003). A Gateway Cloning Vector Set for High-Throughput Functional Analysis of Genes in Planta. Plant Physiol. *133*, 462–469.

94. Takken, F.L.W., Luderer, R., Gabriëls, S.H.E.J., Westerink, N., Lu, R., De Wit, P.J.G.M., and Joosten, M.H.A.J. (2000). A functional cloning strategy, based on a binary PVX-expression vector, to isolate HR-inducing cDNAs of plant pathogens. Plant J. *24*, 275–283.

95. Maekawa, T., Cheng, W., Spiridon, L.N., Töller, A., Lukasik, E., Saijo, Y., Liu, P., Shen, Q.-H., Micluta, M.A., Somssich, I.E., et al. (2011). Coiled-Coil Domain-Dependent Homodimerization of Intracellular Barley Immune Receptors Defines a Minimal Functional Module for Triggering Cell Death. Cell Host Microbe *9*, 187–199.

96. Förderer, A., Li, E., Lawson, A.W., Deng, Y.N., Sun, Y., Logemann, E., Zhang, X., Wen, J., Han, Z., Chang, J., et al. (2022). A wheat resistosome defines common principles of immune receptor channels. Nature *610*, 532–539.

97. Liu, D., Shi, L., Han, C., Yu, J., Li, D., and Zhang, Y. (2012). Validation of reference genes for gene expression studies in virus-infected Nicotiana benthamiana using quantitative real-time PCR. PLoS One *7*, e46451.

98. Onozuka, N., Ohki, T., Oka, N., and Maoka, T. (2021). One-step real-time multiplex reverse transcription-polymerase chain reaction assay with melt curve analysis for detection of potato leafroll virus, potato virus S, potato virus X, and potato virus Y. Virol. J. *18*, 131.

99. Yoo, S.-D., Cho, Y.-H., and Sheen, J. (2007). Arabidopsis mesophyll protoplasts: a versatile cell system for transient gene expression analysis. Nat. Protoc. *2*, 1565–1572.

100. Durocher, Y., Perret, S., and Kamen, A. (2002). High-level and high-throughput recombinant protein production by transient transfection of suspension-growing human 293-EBNA1 cells. Nucleic Acids Res. *30*, E9.

101. Repetto, G., del Peso, A., and Zurita, J.L. (2008). Neutral red uptake assay for the estimation of cell viability/cytotoxicity. Nat. Protoc. *3*, 1125–1131.

Please cite this article in press as: Shen et al., Cytoplasmic calcium influx mediated by plant MLKLs confers TNL-triggered immunity, Cell Host & Microbe (2024), https://doi.org/10.1016/j.chom.2024.02.016

STAR★METHODS

KEY RESOURCES TABLE

REAGENT or RESOURCE	SOURCE	IDENTIFIER
Antibodies		
Rat Monoclonal Anti-HA	Sigma-Aldrich	Cat# 11867423001
Goat Anti-Rat	Sigma-Aldrich	Cat# AP136P
Rabbit Polyclonal Anti-GFP	Abcam	Cat# ab6556
Goat Anti-Rabbit	Sigma-Aldrich	Cat# A9169
Mouse Monoclonal Anti-FLAG	Sigma-Aldrich	Cat# F1804
Goat Anti-Mouse	Sigma-Aldrich	Cat# A9316
Horseradish peroxidase (HRP)-coupled Anti-DYKDDDDK	Miltenyi Biotec	Cat# 130-101-572
Horseradish peroxidase (HRP)-coupled Anti-HA	Miltenyi Biotec	Cat# 130-091-972
Mouse monoclonal Anti- Alpha-Tubulin	Sigma-Aldrich	Cat# T6074
HRP-coupled Anti-mouse	Cell Signaling Technology	Cat# 7076S
Bacterial and virus strains		
Chemically Competent *E. coli*	MPIPZ stock	N/A
Electrically Competent *A. tumefaciens* GV3101 (pMP90RK or pMP90Rgent)	MPIPZ stock	N/A
Pseudomonas syringae pv. *tomato* (*Pst*) DC3000	Mahdi et al.[10]	N/A
Xanthomonas campestris pv vesicatoria (*Xcv* 85-10)	Thieme et al.[87]	N/A
P. fluorescens 0-1 expressing empty vector (Pf0-EV)	Saucet et al.[42]	N/A
P. fluorescens 0-1 expressing AvrRps4 (Pf0-AvrRps4)	Saucet et al.[42]	N/A
P. fluorescens 0-1 expressing AvrRpm1(Pf0-AvrRpm1)	Grant et al.[56]	N/A
P. fluorescens 0-1 expressing XopQ (Pf0-XopQ)	Schultink et al.[43]	N/A
Biological samples		
Arabidopsis thaliana leaves	*Arabidopsis thaliana*	N/A
Arabidopsis thaliana protoplasts	*Arabidopsis thaliana*	N/A
Nicotiana benthamiana leaves	*Nicotiana benthamiana*	N/A
Chemicals, peptides, and recombinant proteins		
Brefeldin A	Sigma-Aldrich	Cat# B6542
Cycloheximide	Sigma-Aldrich	Cat# 239763-M
Chitin (NA-COS-Y)	Mahdi et al.[10]	N/A
Flagellin epitope flg22	MPIPZ stock	N/A
Oryzalin	Sigma-Aldrich	Cat# 36182
Fluo-4 AM	AAT Bioquest	Cat# 20551
FM4-64	Sigma-Aldrich	Cat# SCT127
Critical commercial assays		
RNeasy Plant Mini Kit	QIAGEN	Cat# 74904
4x Laemmli Sample Buffer	Bio-Rad	Cat# 1610747
GFP Selector magnetic beads	NanoTag	Cat# N0310
Experimental models: Cell lines		
Sf21 insect cells	Invitrogen	Cat# 11497013
Human embryonic kidney, HEK293T	ATCC	CRL-3216™
Experimental models: Organisms/strains		
Arabidopsis: Col-0	MPIPZ stock	N/A
Arabidopsis: *mlkl123*	Mahdi et al.[10]	N/A
Arabidopsis: *MLKL1-GFP*	Mahdi et al.[10]	N/A
Arabidopsis: *eds1-12*	Ordon et al.[53]	N/A

(*Continued on next page*)

Please cite this article in press as: Shen et al., Cytoplasmic calcium influx mediated by plant MLKLs confers TNL-triggered immunity, Cell Host & Microbe (2024), https://doi.org/10.1016/j.chom.2024.02.016

CellPress
OPEN ACCESS

Continued

REAGENT or RESOURCE	SOURCE	IDENTIFIER
Arabidopsis: *MLKL1-GFP* in *eds1-12*	This paper	N/A
Arabidopsis: 35S::*Helo-GFP* in *mlkl123*	This paper	N/A
Arabidopsis: 35S::*GCaMP3* in Col-0	Vincent et al.[55]	N/A
Arabidopsis: 35S::*GCaMP3* in *mlkl123*	This paper	N/A
Arabidopsis: 35S::*GCaMP3* in *nrg1.1,1.2*	This paper	N/A
Nicotiana: WT	This paper	N/A
Nicotiana: *eds1a, pad4, sag101a, sag101b*	Lapin et al.[24]	N/A
Nicotiana: 35S::*GCaMP3* in WT	DeFalco et al.[57]	N/A
Oligonucleotides		
See Table S1 for primers	This paper	N/A
Recombinant DNA		
pUC19-AvrRps4-3xFLAG	Xing et al.[88]	N/A
pAMPAT-35S-mClover3	This paper	N/A
pAMPAT-35S-HeLo-mClover3	This paper	N/A
pAMPAT-35S-HeLoBrace-mClover3	This paper	N/A
pAMPAT-35S-HeLoBracePseudokinase-mClover3	This paper	N/A
pAMPAT-35S-*At*MLKL1-mClover3	This paper	N/A
pAMPAT-35S-BracePseudokinaseID-mClover3	This paper	N/A
pAMPAT-35S-HeLo-3xHA	This paper	N/A
pAMPAT-35S-HeLoBrace-3xHA	This paper	N/A
pAMPAT-35S-HeLoBracePseudokinase-3xHA	This paper	N/A
pAMPAT-35S-*At*MLKL1-3xHA	This paper	N/A
pAMPAT-35S-BracePseudokinaseID-3xHA	This paper	N/A
pXCSG-35S-HB-3xHA	This paper	N/A
pXCSG-35S-HP-3xHA	This paper	N/A
pXCSG-35S-HH-3xHA	This paper	N/A
pXCSG-35S-HH+HP-3xHA	This paper	N/A
pXCSG-35S-HP+HB-3xHA	This paper	N/A
pXCSG-35S-S393D-3xHA	This paper	N/A
pSfinx-mYFP	This paper	N/A
pAMPAT-35S-*At*MLKL1-cYFP	This paper	N/A
pESPY-35S-*At*SAG101-nYFP	This paper	N/A
pXCSG-*At*EDS1-FLAG	Lapin et al.[24]	N/A
pXCSG-*At*SAG101-FLAG	Lapin et al.[24]	N/A
pXCSG-*At*NRG1.1-3xHA	Lapin et al.[24]	N/A
pXCSG-GUS-FLAG	Lapin et al.[24]	N/A
pBIN20-35S-GCaMP3	Vincent et al.[55]	N/A
pMDC7-HeLo-3xHA	This paper	N/A
pGWB517-35S-P19	This paper	N/A
pGWB517-35S-CMV2b	This paper	N/A
pcDNA™5/FRT/TO- *Hs*MLKL (HeLo+Brace)-FLAG	This paper	N/A
pcDNA™5/FRT/TO- *At*MLKL (HeLo)-FLAG	This paper	N/A
pcDNA™5/FRT/TO- *At*MLKL (HeLo+Brace)-FLAG	This paper	N/A
Software and algorithms		
Fiji	Schindelin et al.[89]	https://fiji.sc/
R studio	RStudioTeam, 2018	http://www.rstudio.com/
Alfafold2	Jumper et al.[49]	https://alphafold.com/

Please cite this article in press as: Shen et al., Cytoplasmic calcium influx mediated by plant MLKLs confers TNL-triggered immunity, Cell Host & Microbe (2024), https://doi.org/10.1016/j.chom.2024.02.016

RESOURCE AVAILABILITY

Lead contact

Further information and requests for resources and reagents should be directed to and will be fulfilled by the Lead Contact, Takaki Maekawa (tmaekawa@uni-koeln.de).

Materials availability

All unique reagents generated in this study, including plasmid vectors used to generate transgenic plants, are available from the lead contact with a completed Materials Transfer Agreement.

Data and code availability

This paper does not report original code. All the R codes and additional information required to reanalyze the data reported in this paper is available from the lead contact upon request.

EXPERIMENTAL MODEL AND STUDY PARTICIPANT DETAILS

Arabidopsis thaliana and growth conditions

The *Arabidopsis thaliana* complementation line expressing *AtMLKL*1-GFP under the native *cis*-regulatory sequence in *Atmlkl1* background was described previously.[10] Using the floral dip method,[90] *Arabidopsis* Col-0 (wild-type) and the *eds1-12* mutant[53] were transformed by *Agrobacterium tumefaciens* strain GV3101 pMP90RK[91] carrying the above *AtMLKL*1-GFP complementation construct. Similarly, the *Atmlkl123* triple mutant[10] and *Atnrg1.1,1.2* double mutant[24] were transformed by *A. tumefaciens* strain GV3101 pMP90Rgent[91] carrying pBIN20::CaMV35S:GCaMP3.[55] Wild-type *A. thaliana* plants transformed with pBIN20::CaMV35S:GCaMP3 were generated previously.[55] Plant growth conditions were described previously.[41] To screen transgenic Arabidopsis plants, surface-sterilized seeds (washed 3 times with 75% ethanol, followed by washing 4 times with MilliQ water) were sown on half strength Murashige and Skoog agar plates with appropriate antibiotics. MS plates with seeds were placed at 4 °C for 2 days and transferred to growth chambers with following conditions: 10 h light, 14 h dark, 100-150 μmol m^{-2} s^{-1}, 22 °C, 65 % humidity.

Nicotiana benthamiana and growth conditions

N. benthamiana seeds of the wild-type, transgenic line and mutants described in the key resources table were sown on moist soil and covered with a plastic lid until the seeds germinated. *N. benthamiana* plants transformed with pBIN20::CaMV35S:GCaMP3 were generated previously.[57] Plants were grown in a greenhouse chamber under the following conditions: 14 h light, 10 h dark, 100-150 μmol m^{-2} s^{-1}, 23°C, 65% humidity. Plants 4-5 weeks old were used for all experiments.

Pathogen strains and growth conditions

Pseudomonas syringae pv. Tomato DC3000 (*Pst*) DC3000, *Pseudomonas fluorescens* 0-1 (Pf0-1) strain and *Xanthomonas campestris pv. vesicatoria* (Xcv 85-10) described in the key resources table were grown on selective nutrient yeast glycerol agar (NYGA) medium (5 g peptone, 3 g yeast extract, 20 ml glycerol for 1 L, pH 7.0, 1.5 % (w/v) agar for plating) plates with the appropriate antibiotics at 28 °C for 1 day. The selective antibiotic for *Pst* DC3000 cultivation is 100 μg/ml rifampicin. The selective antibiotics for Pf0-EV, Pf0-AvrRPS4 and Pf0-XopQ cultivation are 5 μg/ml tetracycline, 25 μg/ml gentamycin and 30 μg/ml chloramphenicol. The selective antibiotics for Pf0-AvrRpm1 cultivation are 5 μg/ml tetracycline, 50 μg/ml carbenicillin and 25 μg/ml kanamycin. The selective antibiotics for *Xcv* cultivation are 100 μg/ml rifampicin and 150 μg/ml streptomycin. The plates containing the pathogens were kept in a fridge at 4 °C. Before each experiment, bacteria were streaked onto fresh selective NYGA plates and grown overnight.

Agrobacterium tumefaciens growth condition

Agrobacterium cultures were plated on the Yeast Extract Beef (YEB) medium (5 g beef extract, 1 g yeast extract, 5 g peptone, 5 g sucrose, 2 ml $MgSO_4$ (1 M), pH 7.2, 1 % (w/v) agar for plating) plates with the corresponding antibiotics of the plasmid described in the key resources table in an appropriate concentration. Plates were incubated in 28 °C for 2 to 3 days until single colonies were visible.

Human cell and culture conditions

Human embryonic kidney (HEK293T; ATCC® CRL-3216™) cells were cultivated in Dulbecco's Modified Eagle Medium (DMEM; Invitrogen) supplemented with 10% fetal-bovine serum (Gibco) and 1% penicillin-streptomycin (Gibco) and maintained at 37 °C, 95% humidity and 5% CO_2.

METHOD DETAILS

Ca^{2+} imaging in leaves

The GCaMP3 signal was acquired in a temperature-controlled (22°C) dark room by a motorized fluorescence stereo microscope Nikon SMZ25 equipped with a 0.5 x objective lens (SHR Plan Apo, WD:71, Nikon) and a high-resolution Nikon DS-Ri2 camera. GCaMP3 was

excited using a Nikon GFP-BP filter cube, EX: 470/40 and EM: 525/50. Every 5 min, the GCaMP3 signal was acquired and analyzed by the NIS-Elements Advanced Research microscope imaging software. In the figure, data from every 30 min are shown. For the time-lapse measurement for *A. thaliana*, 4–6-week-old plants were used. Immediately after the infiltration of bacterial suspension, the detached leaves were arranged on a piece of black cardboard that was placed over a wet paper tissue before being placed in a plastic Petri dish. After adjustment of exposure time (usually to 5 s), the measurement was started. During the experiment, the Petri dish was closed with a lid. For the image analysis, Fiji software[89] was used to adjust brightness and contrast. Furthermore, for all leaves, an individual Region of Interest (ROI) was defined and fluorescence levels were displayed by 'Plot Z-axis profile'. For the bacterial infiltration, the OD_{600} was adjusted to 0.2 with autoclaved milliQ water. The abaxial sides of the leaves were infiltrated with the bacterial suspension using a 1-ml needleless syringe. The site wounded by the syringe as well as the infiltrated area was marked with a permanent marker.

ß-estradiol-based transient protein expression in *N. benthamiana* for Ca^{2+} imaging

Agrobacterium culture and agroinfiltration were essentially described previously.[92] *A. tumefaciens* strain GV3101 pMP90RK carrying the ß-estradiol-inducible constructs (pMDC7-GW-3xHA[93]) of *At*MLKL1 variants or an empty vector (OD_{600} = 0.8) were co-infiltrated into leaves of *N. benthamiana* expressing GCaMP3[57] with *A. tumefaciens* strain GV3101 pMP90RK carrying pGWB517:: CaMV35S:CMV2b (OD_{600} = 0.2) and pGWB517:35S:P19 (OD_{600} = 0.2). A needleless 1-ml syringe was used for infiltrations. One leaf was infiltrated a maximum of six times, without overlapping infiltration sites. For the ß-estradiol application, the infiltrated leaves were sprayed with 200 μM ß-estradiol solution containing 0.002% [v/v] Silwet L-77 two days after infiltration with *A. tumefaciens*. The GCaMP3 signal was measured as described above. Leaves samples were collected by harvesting five 6-mm leaf-discs using a biopsy punch from the infiltrated areas. The collected leaf discs were snap-frozen using liquid nitrogen and kept in a -80°C freezer until protein extraction.

Immunoblotting (*N. benthamiana*)

For protein extraction in *N. benthamiana*, the samples were ground to fine powder, and 250 μl of urea–SDS extraction buffer (50 mM Tris-HCl pH 6.8, 2% SDS, 8 M urea, 2% β-mercaptoethanol, 5% glycerol) was added to the tube containing the sample powder. All samples were subsequently incubated at room temperature (RT) for 10 min with shaking and without further boiling. The resulting lysate was centrifuged 2 times at 16,000 x g for 10 min at RT. After each centrifugation the supernatant was transferred to a new tube. The protein concentration was determined by a Bradford protein assay using BSA (Thermo Scientific Albumin Standard Kit) as a standard and measuring the absorbance at 600 nm.

The proteins were separated by SDS-PAGE. Electrophoresis was performed at 100 V for 60-90 min, and proteins were transferred to polyvinylidene fluoride (PVDF) membranes. The membranes were then blocked in 5% milk TBS-T for 3 h and incubated overnight at 4°C with the appropriate primary antibody in 5% nonfat dry milk TBS-T. The appropriate horseradish (HRP)-conjugated secondary antibody was applied for 2 h in 5% milk TBS-T. Membrane detection was performed using SuperSignal West Femto Maximum Sensitivity Substrate (Thermo Fisher Scientific) and the ChemiDoc MP imaging system (Biorad). Equal protein transfer was monitored by staining membranes with Ponceau S or Coomassie Brilliant Blue. The following antibodies were used in immunoblot assays: monoclonal rat anti-HA antibody (Sigma Aldrich) diluted 1:4,000, goat anti-rat peroxidase antibody (Sigma-Aldrich) diluted 1:5,000, polyclonal rabbit anti-GFP antibody (Abcam) diluted 1:4,000, goat anti-rabbit peroxidase antibody (Sigma-Aldrich) diluted 1:5,000, monoclonal mouse anti-FLAG antibody (Sigma-Aldrich) diluted 1:3,000, goat anti-mouse alkaline phosphatase antibody diluted 1:5,000 (Sigma-Aldrich).

Immunoblotting (*A. thaliana*)

For protein extraction in *A. thaliana*, the samples were ground to fine powder, and an equal volume of 2x Laemmli Sample Buffer (Bio-Rad) with 10% 2-mercaptoethanol was added to the tube containing the sample powder. All samples were subsequently boiled at 65°C for 10 min. After this, the procedure was the same as described for immunoblotting in *N. benthamiana*.

Pathogen infection assays using YFP-expressing Potato virus X

The monomeric YFP coding region was amplified from pXCSG-YFP[65] by PCR using the primers containing the *SfiI* recognition sites and the PCR product was digested with *Sfi*I (NEB) and ligated into the *Sfi*IA and *Sfi*IB sites of the binary PVX-based expression vector.[94] The resulting plasmid designated as pSfinx-mYFP was transformed into *A. tumefaciens* strain GV3101 pSoup.[94] The coding regions of GUS (Thermo Fisher Scientific), the HH+HP (G12D, A16D, L20D, R74E, S287E, L341E, R370E) variant of *At*MLKL1, the HP+HB (R74E, W93A, I97E, F213E, S287E, L341E, R370E) variant of *At*MLKL1, and the S393D variants of *At*MLKL1 were cloned into pXCSG-3HA[95] using LR Clonase II (Thermo Fisher Scientific) or In-Fusion cloning (Takara Clontech). The resulting plasmids were transformed into *A. tumefaciens* strain GV3101 pMP90RK.[91] The *A. tumefaciens* strain carrying pSfinx-mYFP (OD_{600} = 0.001) and the *A. tumefaciens* strain carrying either GUS or *At*MLKL1 variants (OD_{600} = 0.6) were co-infiltrated into leaves of wild-type, *adr1 nrg1* mutant,[52] or *eds1 pad4 sag101a sag101b* mutant[24] of *N. benthamiana*. The *A. tumefaciens* strains each carrying Sr35 (OD_{600} = 0.075) and AvrSr35 (OD_{600} = 0.5)[96] were used as controls.

At 4 days after infiltration, ten 5-mm leaf discs per condition were collected using a biopsy punch from the infiltrated areas. The collected leaf discs were snap-frozen using liquid nitrogen and kept in a -80 °C freezer until use. The leaf discs were ground using a pestle or Retsch mill, and 200 μl of the extraction buffer (50 mM Tris-HCl pH 8.40, 150 mM NaCl, proteinase inhibitor (Roche: cOmplet, EDTA-free Protease Inhibitor Cocktail)) were added. The resulting lysate was centrifuged at 30,000 x g for 5 min and 80 μl of the

supernatant was loaded into a black 96 well plate (Corning: CLS3915-100EA). The fluorescence microplate reader (TECAN: Tecan infinite 200 pro) was used to measure YFP intensity (excitation: 516 nm and emission: 560 nm). YFP intensity was used as a proxy for PVX viral load.

For correlation analysis between YFP intensity and RNA encoding the coat protein (CP) of PVX, different concentrations of *A. tumefaciens* containing pSfinx-mYFP (OD_{600} = 0.0001, 0.001, 0.01) were infiltrated into the abaxial side of *N. benthamiana leaves*. Four days after infiltration, 20 5-mm leaf discs per condition were collected from the infiltrated leaves, and ten randomly selected leaf discs were used for protein and RNA extraction, respectively. RNA extraction, reverse transcription, and qPCR were performed as previously described.[41] The relative expression of RNA encoding CP was normalized to the *NbF-BOX* gene, which was previously described to be highly constant in virus-infected *N. benthamiana* plants.[97] The gene-specific primers (in 5' to 3' direction) were as follows: *PVX CP* (fw: TTCGACTTCTTCAATGGAGTC, rv: TCCAGTGATACGACCTCG),[98] *NbF-BOX* (fw: GGCACTCACAAACGTCTATTTC, rv: ACCTGG GAGGCATCCTGCTTAT).[97]

Recombinant protein expression in insect cells and size-exclusion analysis

*At*MLKL1 (residues 1–133) with an N-terminal His6-SUMO tag construct in the pFastBac1 vector (Invitrogen) was generated using a standard PCR-based cloning strategy. The protein was expressed in Sf21 insect cells. One litre of cells was infected with 20 ml baculovirus at 28 °C. After 48 h of growth at 28 °C, the cells were harvested and resuspended in a buffer containing 50 mM Tris-HCl pH 8.0 and 300 mM NaCl, and lysed by sonication. The soluble fraction was purified from the cell lysate using cobalt affinity resin (HisPur Cobalt Resin). The protein was subsequently subjected to size-exclusion analysis (Cytiva: Superose 6 Increase 10/300 GL).

Confocal microscopy

Transfected protoplasts in a chamber slide (Nunc Lab-Tek, Thermo Fisher Scientific) with incubation buffer, i.e. WI solution,[99] or 2–6 mm leaf discs prepared from rosette leaves of *Arabidopsis* or *Nicotiana* plants with or without pathogen challenge were observed under a confocal microscope (LSM880, Carl Zeiss, Germany) equipped with a 40x water-immersion and a 63x oil-immersion objective. Lambda stack images were obtained for spectral imaging. Images were analyzed and processed with ZEN Software (Carl Zeiss) and Fiji.[89]

Construction of plasmids with *At*MLKL1 variants

Unless otherwise specified, coding sequences (CDS) of *AtMLKL1* variants without stop codons were initially cloned into pENTR/D-TOPO, pDONR221, or pDONR207 (Thermo Fisher Scientific). For mClover3-tagged *AtMLKL1* variants, *CDS* were cloned into D-TOPO-mClover3 using In-Fusion cloning (Takara Clontech). Entry clones were transferred into the Gateway cloning-compatible pAMPAT-GW-3xHA or pAMPAT-GW expression vectors.[95] The delineation of domain boundaries of *At*MLKL1 is as follows, HeLo: aa 1–133, Brace: aa 134–220, Pseudokinase aa 221–567, Intrinsically disordered (ID) region aa 568–717.

Transient gene expression in protoplasts

Protoplasts were isolated from the leaves of 4-week-old *Arabidopsis thaliana* complementation line expressing *At*MLKL1-GFP under the native cis-regulatory sequence in the *Atmlkl1* background. Transfection was as previously described.[99] The *AvrRps4* gene was fused with the FLAG epitope on the pUC19 vector,[88] kindly provided by Dr. Jane Parker's lab. Immunoblotting was performed as described above.

Bimolecular fluorescence complementation (BiFC) assays

Agrobacteria delivering BiFC constructs *At*EDS1-FLAG (OD_{600} = 0.2), *At*SAG101-nYFP (OD_{600} = 0.2), and *At*MLKL-cYFP (OD_{600} = 0.8) were infiltrated into leaves of *N. benthamiana* quadruple mutant *eds1a pad4 sag101a sag101b* (*Nb-epss*).[24] At 48 hpi, Pf0-XopQ or Pf0-EV (OD_{600} = 0.3) were infiltrated into the same leaf zone. At 6-8 hpi of Pf0-1 strain, leaf discs were used to observe fluorescence under a confocal microscope (LSM880, Carl Zeiss, Germany).

Pathogen infection assays (*Pst* DC3000)

Pseudomonas syringae pv. *tomato* (*Pst*) DC3000 was syringe-infiltrated into *Arabidopsis* leaves at OD_{600} = 0.0005 in 10 mM $MgCl_2$. Bacterial titers were determined at 3 dpi. The released *Pseudomonas* bacteria were diluted and plated onto NYGA plates supplemented with 100 mg/L rifampicin and 25 mg/L kanamycin.

Xanthomonas growth assay in *N. benthamiana*

Xanthomonas campestris pv vesicatoria (*Xcv* 85-10)[87] was kindly provided by Ulla Bonas and Johannes Stuttmann at University of Halle. The *Xcv* growth assays in *N. benthamiana quadruple mutant eds1a pad4 sag101a sag101b (Nb-epss)* in the presence of agrobacteria-delivering proteins *At*EDS1-FLAG (OD_{600} = 0.2), *At*SAG101-FLAG (OD_{600} = 0.2), *At*NRG1-HA (OD_{600} = 0.5) and *At*MLKL-GFP (OD_{600} = 0.8) were performed as described previously.[24,26] *Xcv* strains were syringe-infiltrated into same leaf zone of transient expression protein at OD_{600} = 0.0005 in 10 mM $MgCl_2$. Samples were collected at 6 days after *Xcv* infiltration. The released bacteria were diluted and the dilutions were plated on fresh selective NYGA plates.

Drug treatments

Drugs were used at the following concentrations: 50 μM CHX, 50 μM BFA, 1 mg/ml chitin, 5 mM flg22. *At*MLKL1-GFP seedlings were treated with various mixed working solutions for 1 h. Before observation under a confocal microscope (LSM880, Carl Zeiss, Germany), samples were immersed in 10 μM FM4-64 for 10 min. Plasmolysis was induced by 0.8 M mannitol for 25 min.

Immunoprecipitation assays

Protein was purified from 1.0 g infiltrated *N. benthamiana* leaves. Samples were ground to fine powder by a mortar and pestle in liquid nitrogen. Then, 2 ml of extraction buffer (10% glycerol, 50 mM Tris-HCl pH 7.5, 5 mM $MgCl_2$, 150 mM NaCl, 10 mM DTT, 0.25% NP-40, 0.25% TritonX-100, 0.6 mM PMSF, 20 mM MG132, 1x Plant protease cocktail (11873580001, MilliporeSigma)) were added. Lysates were incubated on ice for 10 min and were centrifuged for 10 min at 13000 × *g*, two times. The 50 μl aliquots of the filtered supernatant were taken as input samples. Co-IPs were conducted for 2 h with 20 μl GFP magnetic beads (NanoTag) under constant rotation. Beads were washed 4 times in wash buffer (same as extraction buffer but without DTT, PMSF, MG132 and 50mM NaCl). Immunoblotting was performed as described for immunoblotting in *N. benthamiana*.

Plasmid construction for protein expression in human cell culture

The expression constructs of the C-terminally FLAG-tagged *Hs*MLKL (HeLo+Brace) and *At*MLKL1 truncations (Helo only, HeLo+Brace, and full length) were generated by PCR in combination with In-Fusion cloning (Takara Clontech). Phusion DNA Polymerase (New England Biolabs) was used for PCR. For protein expression in human cell culture, all purified PCR products were cloned into the pcDNA5/FRT/TO vector (ThermoFisher) together with the purified CIUDAD PCR construct (unpublished, AG Hofmann, Figure 4E) using In-Fusion (Takara Clontech).

Plasmid transfection into HEK293T cells

HEK293T cells were transfected using PEI.[100] In brief, 1 μg/μl (PEI: DNA = 2.5:1) transfection mix was added in DMEM supplemented with 5% FBS and 0.5% antibiotics to the cells. Transfection reagent was replaced with DMEM (10% FBS and 1% antibiotics) 5 h after transfection.

Immunoblotting (human cells)

HEK293T cells were lysed in 1x Laemmli sample buffer (125 mM Tris-HCl, pH 6.8, 20% glycerol, 4% SDS, 0.03% bromophenol blue, 20 μl/ml ß-mercaptoethanol). The whole-cell lysates were sonicated, boiled for 10 minutes, and then proteins were resolved by sodium dodecyl sulfate-polyacrylamide gel electrophoresis (SDS-PAGE). After transfer of separated proteins onto PVDF membranes, membranes were blocked in 5% blocking solution (5% milk powder in PBS-T) and then probed for FLAG, HA and tubulin using horseradish peroxidase (HRP)-coupled anti-DYKDDDDK antibody (Miltenyi Biotec), horseradish peroxidase (HRP)-coupled anti-HA antibody (Miltenyi Biotec), anti-alpha-tubulin (Sigma Aldrich) and the appropriate HRP-coupled anti-mouse antibody (Cell Signaling Technology). Proteins were detected using enhanced chemiluminescence (ECL; Biozym WesternBright) and signals were collected using GelDoc Imager (BioRad).

Live-cell cytoplasmic Ca^{2+} imaging in human cells

HEK293T cells were seeded into 48 well plates (VWR; 10062-898) and transfected 24 h before live-cell imaging. The medium was supplemented with 1 μM Fluo-4-AM (AAT Bioquest) a cell-permeable fluorescent Ca^{2+} indicator. Fluo-4 with the AM group is able to cross PM by diffusion and intracellular esterases cleave the AM group and trap the dye inside cells. Ca^{2+} binding enhances the fluorescence of Fluo-4. Directly before the measurement, 5 μg/ml rapamycin (Apollo Scientific; 53123-88-9) were added to the transfected cells. Cytoplasmic calcium ions were measured with IncuCyte S3 live-cell imaging. Cells were imaged using the 10x objective and bright field, green, and red channel settings. Cytoplasmic calcium ions were measured at 10-min intervals. Analysis was performed in Excel by calculating the mean and the standard error of the replicates.

Cell viability assay in human cells

For cell viability assays, HEK293T cells were seeded in 48-well plates and transfected with the various *At*MLKL plasmids. 24 h after transfection, 5 μg/ml rapamycin were added and after a further 24 h the neutral red assay[101] was performed. In brief, 40 μg/ml neural red solution (Fluka; 553-24-2) were added to the cells followed by incubation for 2–3 h at 37 °C, 95% humidity and 5% CO_2. Neural red solution was aspirated, cells were washed once with 1x PBS, and destaining solution (50% ethanol, 1% glacial acetic acid) was added. To extract the neural red, the plate was placed onto a rocker for at least 15 minutes. To evaluate cell viability, the absorbance of neutral red extract at 540 nm was measured in a plate reader (TECAN Infinite F200Pro).

QUANTIFICATION AND STATISTICAL ANALYSIS

ANOVA with Turkey's HSD test, one sample *t*-test and two-tailed student's *t*-test were used to determine statistical significance as indicated in the respective figure legends, unless otherwise specified. The exact number of experimental replicates was noted in the corresponding figure legends.